VISCID-INVISCID FLOW INTERACTIONS

by

KING-MON TU

A dissertation submitted to the Graduate Faculty in Engineering in partial fulfillment of the requirement for the degree of Doctor of Philosophy, The City University of New York.

1974

This manuscript has been read and accepted for the Graduate Faculty in Engineering in satisfaction of the dissertation requirement for the degree of Doctor of Philosophy.

1/24/75 — Date

Sheldon Weinbaum — Chairman of Examining Committee

1/27/75 — Date

Jacques E. Benveniste — Executive Officer

Thomas A. Hewett

Norman C. Jen

Myron Levitsky

Robert Melnik

Chan Mou Tchen

Sheldon Weinbaum, Chairman

Supervisory Committee

The City University of New York

Acknowledgements

I wish to express my sincere appreciation to my mentor Dr. Sheldon Weinbaum for his guidance and for sharing with me his profound understanding of the mathematical and physical sciences throughout the course of study which has culminated in this research effort. I also wish to thank my Doctoral Committee members, Professor Robert F. Dressler, Professor Thomas A. Hewett, Professor Norman C. Jen, Professor Myron Levitsky, Dr. Robert Melnik and Professor Chan Mou Tchen, for their interest and effort. I would like to express my appreciation to The City College and The City University of New York for the financial assistance which they gave me during my graduate career.

Dedication

to

My Parents and My Wife

Table of Contents

List of Figures

Abstract

This investigation presents an approximate non-asymptotic theory for self-sustaining supersonic laminar boundary layer interaction which is based on the three layer conceptual model first introduced by Lighthill (1953) to explain the upstream propagation of disturbances in linear shock wave boundary layer interactions where separation does not occur and recently extended by Stewartson and Williams (1969) (1973) for non-linear interactions with separation using an asymptotic analysis valid for infinite R_e . The practical shortcoming of the asymptotic analysis is that at the largest R_e for which the boundary layer could be expected to remain laminar the viscous sublayer whose thickness is of $O(R_e^{-\frac{1}{8}} \delta)$ is of comparable thickness to the inviscid interaction layer and thus not a thin sublayer as required for the validity of an asymptotic theory. This investigation extends the basic three layer model for laminar boundary layer free interaction phenomena to physically realizable flows in the Reynolds number range $10^4 \leq R_e \leq 10^6$ where the viscous sublayer can not be viewed as thin in an asymptotic sense. Both major shortcomings of the lowest order asymptotic analysis, the neglect of the streamtube divergence in the inviscid interaction layer and compressibility effects in the viscous sublayer, are considered in the present analysis. Another novel feature of this study is the separation pressure criterion used to determine the effective edge of the laminar viscous sublayer.

The mathematical treatment of each layer is as follows: the external supersonic main stream outside the basic boundary layer is described by a Prandtl-Meyer simple wave relation, the free interaction zone is represented by a continuous distribution of rotational inviscid stream-tubes, and the inner viscous sublayer adjacent to the wall is approximated by a momentum integral of the conventional compressible boundary layer equation which takes into account the novel outer edge conditions for a viscous layer with non-vanishing gradients and the wall compatibility conditions as required by the non-adiabatic boundary layer equations.

Numerical solutions are presented for shock and wedge induced separation phenomena over adiabatic walls for Mach numbers in the range $2 \lesssim M_\infty \lesssim 10$. The distribution of pressure, skin friction and the development of the velocity and enthalpy profiles throughout the interaction region are obtained and are in good agreement with the experimental measurements. This agreement is far superior to the lowest order asymptotic analysis. One of the interesting new results is the gradual shift from the triple deck to the single layer description as the Mach number increases. The possibility of supercritical behavior in highly cooled boundary layers is also studied. Present results suggest that the displacement growth of the sublayer should for all practical flow situations dominate the supercritical behavior of the inviscid interaction layer.

1 Introduction

The study of viscid-inviscid interaction in a compressible boundary layer adjacent to a solid surface has been the subject of numerous theoretical and experimental investigations of the behavior of real fluids in high speed flights. These investigations have shown that the self-sustaining adverse pressure gradient generated by the displacement interaction between the boundary layer and the outer flow can cause a significant modification of the behavior for both the boundary layer and the inviscid external flow. This modification is particularly important if the adverse pressure gradient generated by the displacement interaction is sufficiently large to lead to separation. In these circumstances the inviscid outer flow departs significantly from the description of ideal compressible flow theory and depends on the detailed development of the viscous layer. These modifications which affect the whole interaction flow field occur over a wide range of Reynolds numbers and Mach numbers and are of considerable practical importance in the performance and design of supersonic and hypersonic vehicles. A common application in external aerodynamics is the compression corner resulting from a reflected flap control surface. An important application in internal aerodynamics is the interaction of the leading edge shock wave with the wall boundary layer in the intake of an engine inlet system.

1-1 Qualitative features of the shock wave and wedge induced free interactions

Self-sustaining compressive interactions can be triggered by a variety of downstream disturbances the two most common being the pressure rise due to a shock wave and a compression corner. The first experimental observations of shock wave boundary layer interaction were probably made by early investigators studying the imbedded supersonic region in the transonic flow past an airfoil see for example Ackeret, Feldman and Rott (1946). Some representative more recent experimental investigations include: Liepmann (1946), Gadd (1957), Chapman, Kuehn and Larsen (1958), Hakkinen, Greber, Trilling and Abarbanel (1959), Sterrett and Emery (1960), Miller, Hijman and Childs (1964), Needham (1965), Green (1969) and Lewis, Kubota and Lees (1969).

The two basic typical interaction phenomena are shown schemetically in figures 1 and 2. Figure 1 shows the shock induced interaction produced by an externally generated oblique shock incident on a wall with a well established boundary layer. Figure 2 shows the boundary layer separation and reattachment regions produced by a wedge induced interaction.

A cursory examination of the two figures shows that the two interaction phenomena are qualitatively similar in many respects. In both interactions an adverse pressure gradient is generated by a compressive downstream disturbance which propagates upstream through the subsonic portion of the boundary layer. The adverse pressure gradient causes boundary layer thickening and results in an outward displacement of the external inviscid flow which in turn produces a further steepening of the adverse

pressure gradient. In this manner the flow behavior for both the boundary layer and the external inviscid flow are mutually modified by each other as the interaction proceeds.

The intriguing feature that has been well documented experimentally is that the behavior of a laminar boundary layer separating from the surface far upstream of the main shock impingement point is nearly identical to the behavior of the flow separating far ahead of a wedge in the wedge induced interaction. As Stewartson and Williams (1969) have shown the separation process itself is regular for a supersonic free interaction. The compression waves generated by the displacement interaction of the separating viscous layer coalesce and form a separation shock in the main stream. The strength of this shock wave depends on the wall and free stream conditions upstream of separation and is independent of the nature of the downstream compressive disturbance.

For strong disturbances with extended separated flow regions an interaction zone of approximately constant pressure is established, whereas for weaker disturbances where the boundary layer remains attached or is separated for only short distances no pressure plateau is achieved.

In the case of shock induced interaction the impinging shock wave is first refracted by the Mach number profile of the supersonic portion of the attached or separated boundary layer and then reflected as an expansion fan at the sonic line since the subsonic flow can not support a sudden pressure rise (this reflection process is similar to shock reflection from a free surface in an inviscid flow field). The effect of the shock reflection is to turn the flow near sonic line back towards the wall with an angle which is twice the deflection angle of the local oblique shock. In the case of wedge induced interaction an expansion wave is not required since the flow is already directed towards the wall.

As the free shear layer approaches the reattachment point, it begins to turn parallel to the solid surface causing a strong interaction between the boundary layer and the inviscid external flow. The compression waves produced in this region then coalesce to from the reattachment shock in the main stream. Downstream of the reattachment point the boundary layer displacement thickness reaches a local minimum in the neck region and then relaxes gradually to a self-similar Blasius behavior.

The mathematical model proposed herein is applicable in both shock induced and wedge induced interactions where the separated flow region is too short for a pressure plateau to be established. For reasons to be discussed later this limitation can be removed once a more accurate description of the velocity profiles for the viscous sublayer in the separated flow region are developed.

1-2 Previous theoretical investigations

Theoretical investigations of self sustaining free interacting flow differ fundamentally from classical Prandtl boundary layer theory in that the static pressure field can not be treated as a given datum but has to be determined from the simultaneous solution of the equations governing the viscous and inviscidly behaving fluid regions. The first rational theory attempting to explain the intriguing phenomena of upstream influence and self sustaining interaction in supersonic boundary layers was proposed by Lighthill (1953). In his now classic paper on a linear theory for the growth of small pressure disturbances in a supersonic boundary layer flow without separation Lighthill hypothesized that in the region of strong pressure interaction both laminar and turbulent boundary layer could be divided into three regions of distinctly different behavior: an external supersonic inviscid mainstream outside the basic boundary layer flow, a free interaction zone which extends over the majority of the boundary layer and behaves as an inviscid interacting flow, and a relatively thin inner viscous sublayer adjacent to the wall where the conventional incompressible boundary layer equations apply. The development of a rational non-linear theory capable of describing larger pressure disturbances with separation based on Lighthill's three layer conceptual model has proved to be formidable. The basic difficulties were: (1) the absence of a rational theory for defining the viscous sublayer edge, (2) the fact that the coupling between the viscous sublayer and the inviscid interaction layer occurred in a region close to the wall where normal gradients of velocity and temperature profiles were large and (3) the difficulty in adequately describing a viscous sublayer with reverse flow

and novel outer edge matching conditions in which both viscous and inertia effects are equally important.

Because of the above mentioned difficulties, many investigators chose not to pursue the fundamental three layer conceptual model but to treat the boundary layer as a single layer using either finite difference techniques, Reyhner and Flugge-Lotz (1968), or momentum and energy integral techniques, Lees and Reeves (1964), Holden (1965), Goodwin et al. (1967), Klineberg and Lees (1969). For adiabatic laminar boundary layers at low and moderate supersonic Mach numbers these single layer models provided very encouraging agreement with the experiments. For non-adiabatic and high Mach number laminar boundary layers and for turbulent boundary layers in general the single layer models provided much less satisfactory agreement with experiment and led to important conceptual anomalies. For example, these single layer model theories predict that turbulent and highly cooled laminar boundary layers are supercritical in nature and thus are stable with respect to small pressure disturbances. These supercritical boundary layers according to the theory of Lees and coworkers can not be triggered into a self sustaining displacement interaction unless one permits physically spurious discontinuous supercritical-subcritical jumps. Our present work indicates that the origin of this difficulty stems from the inability of the single layer integral method to adequately describe the viscous sublayer. At very high Reynolds numbers the sublayer should in theory comprise a very small portion of the total boundary layer. The details of the viscous sublayer are thus lost in an integral averaging procedure which is applied across the entire boundary layer and it is somewhat surprising that the single layer integral theories provide the good agreement that they do. In the single

layer analysis of Lees and coworkers the description of the viscous sublayer is further altered by using profiles based on the self similar solutions of the compressible boundary layer equations. The velocity and enthalpy profiles are thus uncoupled from the local streamwise pressure gradient and do not satisfy the other wall compatibility conditions. The theory developed in this study also uses an integral momentum approach but confines the integral averaging to the sublayer region only and satisfies the wall compatibility conditions required by the exact equations for the viscous sublayer. At high Mach numbers these single layer theories become a poor representation because of their inability to adequately describe the wave interaction effects in the inviscidly behaving portion of the boundary layer. These effects are particularly important downstream of shock impingement where both the incident shock and the reflected expansion fan are significantly refracted by the Mach number profile of the undisturbed boundary layer.

Gadd (1957) was the first to attempt to apply the three layer model concept to non-linear boundary layer interactions. His approximate analysis is based on a generalization of Stratford's (1954) model for the behavior of an incompressible boundary layer in the presence of a strong adverse pressure gradient to compressible boundary layer flow. A third order polynomial is used to describe the inner viscous layer and the Bernoulli equation applied along streamlines in the inviscid interaction layer. The junction between the inner viscous and the outer inviscid layers is a function of x and is determined by compatibility conditions that derive from the continuity of the mass flow and its first two derivatives at the edge of the viscous layer. The numerical calculation of the pressure variation up to separation and slightly beyond are in good agreement

with experiment for an adiabatic wall for moderate Reynolds numbers in the range 0.4×10^5 to 0.6×10^6 and Mach numbers of 2 and 4 . The model provided poor agreement with experiment in the separated flow region and could not be continued through reattachment. The principal weaknesses of the model would appear to be the inadequate velocity profile description in the separated flow region and the assumption that the flow inclination at the edge of the sublayer and the edge of the boundary layer are equal.

In the past few years there has been a greatly renewed interest in the development of a non-linear theory pursuing the more rational three region conceptual model proposed by Lighthill (Neiland 1971, Belcher, Burggraf and Stewartson 1972). Stewartson and Williams (1969, 1973) have presented an elegant asymptotic analysis valid in the limit of infinite R_e for an adiabatic laminar boundary layer. The asymptotic analysis circumvents the difficult question of accurately defining the sublayer edge for finite Reynolds numbers but shows that the sublayer thickness is of $O(R_e^{-1/8} \delta)$, that the extent of upstream influence is of $O(R_e^{1/8} \delta)$ and that the normal pressure gradients are only of $O(R_e^{-1/4})$ in the free interaction layer. Unfortunately even at a Reynolds number of 10^6 , the largest R_e for which the boundary layer could reasonably be expected to remain laminar, the sublayer thickness ϵ is about $1/5\ \delta$, assuming the proportionality constant is near unity. This is hardly a small number in an asymptotic sense and it is not surprising that the single layer theories provide better agreement with experiments at moderate Mach numbers in the range $10^4 \leqslant R_e \leqslant 10^6$ than an asymptotic analysis which is strictly valid for infinite R_e . This does not imply that the three layer model is invalid for laminar boundary layers with $10^4 \leqslant R_e \leqslant 10^6$,

but rather that the merging of the sublayer with the free interaction layer is gradual, that the effective edge of the sublayer has to be more clearly defined than in an order of magnitude sense and that the sublayer may be too thick to be treated as an incompressible viscous layer. These hypotheses are borne out by the results of the present study.

While a relatively thick viscous sublayer might be anticipated for laminar boundary layers one would expect the sublayer in a turbulent boundary layer to be considerably thinner, at most a few percent of a boundary layer thickness. Anticipating a very large inviscidly behaving region Rose et al. (1968) have proposed a purely inviscid model for the turbulent shock wave boundary layer interaction in which the inner viscous sublayer is neglected entirely and the wall treated as a horizontal frictionless boundary . An elaborate method of characteristics program with imbedded shocks was written. While this program could obviously not be used to describe the free interaction phenomenon leading to separation or provide results for skin friction and heat transfer, the characteristics calculation did clearly show that the extended pressure rise downstream of the shock impingement was due to the refraction of the incident shock by the boundary layer Mach number profile and the reflection of the ensuing refracted wave system. In a later paper, Rose (1970) an attempt is made to include in an ad hoc manner the important effect of the viscous displacement interaction near the wall. A boundary layer free interaction program for the inner viscous sublayer was combined with the method of characteristics program described above for the inviscid wave interaction region. The two programs were run in an iterative fashion

in an attempt to obtain a converged solution for the sublayer edge and the streamwise pressure distribution. Satisfactory agreement could only be obtained for essentially the same laminar flow situations where the single layer laminar boundary layer programs had already provided good agreement. There appear to be two fundamental difficulties with this very expensive brute force approach. First, the interaction between the sublayer and the inviscidly behaving layer develops as a local rather than a global coupling in which each layer affects the other as the interaction proceeds. Second, the formulation of the boundary layer program for the sublayer is more subtle than can be handled by the standard boundary layer momentum integral derivation. While the Bernoulli equation does apply at the edge of the viscous layer the temperature and velocity gradients at the edge do not vanish as in the usual boundary layer formulation. Thus, both the velocity and temperature profiles and the governing equations differ from the ordinary integral average boundary layer equations and their associated velocity and temperature profiles.

In the next section, the proper formulation of this new boundary value problem is presented. This new mathematical model is only slightly more difficult to solve than the boundary value problem for the existing single layer theories.

1-3 The comparison between an interacting wake flow and an interacting body boundary layer

An important problem related to the interacting boundary layer is the interacting free shear layer in wake flows. Weinbaum and Garvine (1969), (1970) have shown that it is possible within the framework of a rational theory to treat the entire viscous layer in a laminar supersonic wake downstream of reattachment as a single region and thus divide the reattached wake into an inner viscous and outer inviscid stream. The basic difference between the two flows arises from the difference in boundary conditions that apply at $y = 0$, the wall or wake symmetry axis. Wake flows do not in general satisfy a compatibility condition at $y = 0$ relating the pressure and shear stress gradient. Thus in wake flows both the velocity and enthalpy profiles can be expressed as a regular power series in the normal coordinate y and the coefficients of this series expansion chosen freely independent of the local pressure gradient. This being the case one can show that integral of the continuity equation across the shear layer when coupled with the Prandtl-Meyer relation for the outer flow leads to a unique local expression for the streamwise pressure gradient except at a throat or critical point where two solutions exist. In contrast, for a body boundary layer flow the velocity and enthalpy profiles are directly coupled to the local pressure gradient through the compatibility conditions between the streamwise pressure gradient and the gradient of

the wall shear as required by the boundary layer equation of motion. Thus the development of the interaction flow field depends both on the location of the lower boundary of the free interaction zone and on the local value of the streamwise pressure gradient. Another important difference is that a body boundary layer flow is in general non-adiabatic. This requires that the stagnation enthalpy profile like the velocity profile satisfy wall compatibility conditions that derive from the boundary layer energy equation.

2 Mathematical formulation

2-1 Dimensionless equations and coordinates scaling

In this sub-section we present a rational order of magnitude analysis justifying the hypothesis cited in the introduction that an interacting supersonic boundary layer can be treated as two distinct regions, a free interaction zone and an inner viscous sublayer, with different behavior interacting with a third region, an inviscid outer flow. The fundamental equations of motion applied to a compressible viscous fluid flow are the continuity and Navier-Stokes equations. In the present study we consider two dimensional steady state compressible viscous fluid flow neglecting buoyancy forces. The governing equations are as follows:

Continuity:

$$\frac{\partial(\rho u)}{\partial x} + \frac{\partial(\rho v)}{\partial y} = 0 \qquad (1)$$

Momentum x direction:

$$\rho u \frac{\partial u}{\partial x} + \rho v \frac{\partial u}{\partial y} = -\frac{\partial p}{\partial x} + \frac{\partial}{\partial y}\left[\mu\left(\frac{\partial u}{\partial y} + \frac{\partial v}{\partial x}\right)\right]$$

$$+ \frac{\partial}{\partial x}\left\{\mu\left[2\frac{\partial u}{\partial x} - \frac{2}{3}\left(\frac{\partial u}{\partial x} + \frac{\partial v}{\partial y}\right)\right]\right\} \qquad (2)$$

or

$$\rho u \frac{\partial u}{\partial x} + \rho v \frac{\partial u}{\partial y} = -\frac{\partial p}{\partial x} + \frac{4}{3}\frac{\partial}{\partial x}\left(\mu \frac{\partial u}{\partial x}\right) \qquad (3)$$

$$- \frac{2}{3}\frac{\partial}{\partial x}\left(\mu \frac{\partial v}{\partial y}\right) + \frac{\partial}{\partial y}\left(\mu \frac{\partial u}{\partial y}\right) + \frac{\partial}{\partial y}\left(\mu \frac{\partial v}{\partial x}\right)$$

Momentum y direction:

$$\rho u \frac{\partial v}{\partial x} + \rho v \frac{\partial v}{\partial y} = -\frac{\partial p}{\partial y} + \frac{\partial}{\partial x}\left[\mu\left(\frac{\partial u}{\partial y} + \frac{\partial v}{\partial x}\right)\right] + \frac{\partial}{\partial y}\left\{\mu\left[2\frac{\partial v}{\partial y} - \frac{2}{3}\left(\frac{\partial u}{\partial x} + \frac{\partial v}{\partial y}\right)\right]\right\} \quad (4)$$

or

$$\rho u \frac{\partial v}{\partial x} + \rho v \frac{\partial v}{\partial y} = -\frac{\partial p}{\partial y} + \frac{4}{3}\frac{\partial}{\partial y}\left(\mu \frac{\partial v}{\partial y}\right) - \frac{2}{3}\frac{\partial}{\partial y}\left(\mu \frac{\partial u}{\partial x}\right) + \frac{\partial}{\partial x}\left(\mu \frac{\partial u}{\partial y}\right) + \frac{\partial}{\partial x}\left(\mu \frac{\partial v}{\partial x}\right) \quad (5)$$

Energy equation:

$$\rho C_p \left(u \frac{\partial T}{\partial x} + v \frac{\partial T}{\partial y}\right) = u \frac{\partial p}{\partial x} + v \frac{\partial p}{\partial y} + \frac{\partial}{\partial x}\left(K \frac{\partial T}{\partial x}\right) + \frac{\partial}{\partial y}\left(K \frac{\partial T}{\partial y}\right) + 2\mu\left[\left(\frac{\partial u}{\partial x}\right)^2 + \left(\frac{\partial v}{\partial y}\right)^2\right] + \left(\frac{\partial v}{\partial x} + \frac{\partial u}{\partial y}\right)^2 \mu - \frac{2}{3}\mu\left(\frac{\partial u}{\partial x} + \frac{\partial v}{\partial y}\right)^2 \quad (6)$$

Introducing the enthalpy

$$h = C_p T \quad (7)$$

We can rewrite the energy equation (6) in the form

$$\rho u \frac{\partial h}{\partial x} + \rho v \frac{\partial h}{\partial y} = u \frac{\partial p}{\partial x} + v \frac{\partial p}{\partial y} + \frac{\partial}{\partial x}\left(\frac{\mu}{P_r}\frac{\partial h}{\partial x}\right) + \frac{\partial}{\partial y}\left(\frac{\mu}{P_r}\frac{\partial h}{\partial y}\right) + 2\mu\left[\left(\frac{\partial u}{\partial x}\right)^2 + \left(\frac{\partial v}{\partial y}\right)^2\right] + \mu\left(\frac{\partial v}{\partial x} + \frac{\partial u}{\partial y}\right)^2 - \frac{2}{3}\mu\left(\frac{\partial u}{\partial x} + \frac{\partial v}{\partial y}\right)^2 \quad (8)$$

The equation of state for an ideal gas is

$$P = \rho R T = \rho h \frac{\gamma - 1}{\gamma} \quad (9)$$

(all symbols are defined in appendix A)

The conceptual three layer model first proposed by Lighthill (1953) on heuristic grounds can be formally deduced from the relative order of magnitude of various terms in the above equations. By suitably non-dimensionalizing these equations in the sublayer and free interaction layer, one can show that certain terms are smaller than others. By neglecting these small terms, the desired simplification of the governing equations in each layer can be obtained.

As the first step towards the present order of magnitude non-dimensionalization analysis one leaves the thickness of the sublayer ϵ undetermined by introducing an unknown parameter K in the scaling of the y coordinate. We set $\epsilon = I\ L\ R_e^{-K}$ and determine K and I afterwards by requiring that all three regions be compatible.

The characteristic scaling of the x, y coordinates and the u, v velocity components in the free interaction zone is determined next. The characteristic y coordinate is the boundary layer thickness δ. δ is set equal to $E\ L\ R_e^{-\frac{1}{2}}$, where E is obtained from Cohen and Reshotko (1959) and can be expressed as follows:

$$E = \sqrt{2}\int_0^{\eta_\delta} \frac{T}{T_e}\, d\eta \tag{10}$$

The characteristic x coordinate depends on the inverse logarithmic decrement of upstream influence according to Lighthill (1959)

$$\frac{M_e^2}{\sqrt{M_e^2-1}} \int_\epsilon^\delta \frac{1-M^2}{M^2}\, dy \tag{11}$$

where the integral is performed across the inviscidly behaving portion of the boundary layer. If a linear Mach number profile is assumed across the boundary layer a qualitatively reasonable approximation for equation (11) is (see derivation in appendix B)

$$\frac{M_e^2}{\sqrt{M_e^2-1}} \int_{\epsilon}^{\delta} \frac{1-M^2}{M^2} dy = \frac{L E^2}{I} \frac{Re^{k-1}}{\sqrt{M_e^2-1}} \qquad (12)$$

The appropriate characteristic u velocity component for the free interaction zone is based on the u velocity component at the sublayer edge u_ϵ . The correct order for u_ϵ can be estimated from

$$\frac{u_\epsilon}{u_e} = O\left(\frac{\epsilon}{\delta}\right)$$

$$u_\epsilon \approx u_e \frac{I}{E} Re^{-k+\frac{1}{2}} \qquad (13)$$

The characteristic v component is determined from the continuity equation by requiring that the two mass conservation terms should be of the same order of magnitude

$$v_\epsilon \approx u_e \sqrt{M_e^2-1}\, \frac{I^2}{E^2} Re^{-2k+1} \qquad (14)$$

Thus, in the free interaction zone, one introduces the following characteristic reference parameters:

$$x_c = \frac{L Re^{k-1}}{\beta} \frac{E^2}{I} \qquad y_c = \epsilon L Re^{-\frac{1}{2}}$$

$$u_c = u_e \frac{I}{E} Re^{-k+\frac{1}{2}} \qquad v_c = u_e \frac{I^2}{E^2} \beta Re^{-2k+1} \qquad (15)$$

$$\rho_c = \rho_e \qquad u_c = u_e$$

$$P_c = \rho_c u_c^2 \qquad h_c = u_c^2$$

where $\beta = \sqrt{M_e^2 - 1}$ (16)

In the sublayer region, by similar arguments, one can introduce the following characteristic reference parameters:

$$x_c = \frac{E^2}{I}\frac{L}{\beta}Re^{K-1} \qquad y_c = IL\,Re^{-K}$$

$$u_c = u_e \frac{I}{E} Re^{-K+\frac{1}{2}} \qquad v_c = u_e \beta\, Re^{-3K+\frac{3}{2}}$$

(17)

$$\rho_c = \rho_w \qquad u_c = u_w$$

$$P_c = \rho_c u_c^2 \qquad h_c = h_w$$

Introducing the above two sets of characteristic reference variables into equations (3) and (5) using the star (*) symbol to denote a dimensionless variable one obtains for the sublayer:

x direction:

$$\rho^* u^* \frac{\partial u^*}{\partial x^*} + \rho^* v^* \frac{\partial u^*}{\partial y^*} = -\frac{\partial p^*}{\partial x^*} + \frac{4}{3}\frac{\partial}{\partial x^*}\left(u^*\frac{\partial u^*}{\partial x^*}\right)\frac{\mu_c}{\rho_c u_c x_c}$$
$$- \frac{2}{3}\frac{\partial}{\partial x^*}\left(u^*\frac{\partial v^*}{\partial y^*}\right)\frac{\mu_c}{\rho_c u_c x_c} + \frac{\partial}{\partial y^*}\left(u^*\frac{\partial u^*}{\partial y^*}\right)\frac{\mu_c}{\rho_c u_c x_c}\frac{x_c^2}{y_c^2}$$
$$+ \frac{\partial}{\partial y^*}\left(u^*\frac{\partial v^*}{\partial x^*}\right)\frac{\mu_c}{\rho_c u_c x_c} \qquad (18)$$

y direction:

$$\rho^* u^* \frac{\partial v^*}{\partial x^*} \frac{y_c}{x_c} + \rho^* v^* \frac{\partial v^*}{\partial y^*} \frac{y_c}{x_c} = -\frac{\partial p^*}{\partial y^*} \frac{x_c}{y_c} \tag{19}$$

$$+ \frac{4}{3} \frac{\partial}{\partial y^*} \left(\mu^* \frac{\partial v^*}{\partial y^*} \right) \frac{\mu_c}{\rho_c u_c x_c} \frac{x_c}{y_c} - \frac{2}{3} \frac{\partial}{\partial y^*} \left(\mu^* \frac{\partial u^*}{\partial x^*} \right) \frac{\mu_c}{\rho_c u_c x_c} \frac{x_c}{y_c}$$

$$+ \frac{\partial}{\partial x^*} \left(\mu^* \frac{\partial u^*}{\partial y^*} \right) \frac{\mu_c}{\rho_c u_c x_c} \frac{x_c}{y_c} + \frac{\partial}{\partial x^*} \left(\mu^* \frac{\partial v^*}{\partial x^*} \right) \frac{\mu_c}{\rho_c u_c x_c} \frac{y_c}{x_c}$$

and for the free interaction layer:

x direction:

$$\rho^* u^* \frac{\partial u^*}{\partial x^*} + \rho^* v^* \frac{\partial u^*}{\partial y^*} = -\frac{\partial p^*}{\partial x^*} \tag{20}$$

$$+ \frac{4}{3} \frac{\partial}{\partial x^*} \left(\mu^* \frac{\partial u^*}{\partial x^*} \right) \frac{\mu_c}{\rho_c u_c x_c} - \frac{2}{3} \frac{\partial}{\partial x^*} \left(\mu^* \frac{\partial v^*}{\partial y^*} \right) \frac{\mu_c}{\rho_c u_c x_c}$$

$$+ \frac{\partial}{\partial y^*} \left(\mu^* \frac{\partial u^*}{\partial y^*} \right) \frac{\mu_c}{\rho_c u_c x_c} \frac{x_c^2}{y_c^2} + \frac{\partial}{\partial y^*} \left(\mu^* \frac{\partial v^*}{\partial x^*} \right) \frac{\mu_c}{\rho_c u_c x_c}$$

y direction:

$$\rho^* u^* \frac{\partial v^*}{\partial x^*} \frac{y_c}{x_c} + \rho^* v^* \frac{\partial v^*}{\partial y^*} \frac{y_c}{x_c} = -\frac{\partial p^*}{\partial y^*} \frac{x_c}{y_c} \tag{21}$$

$$+ \frac{4}{3} \frac{\partial}{\partial y^*} \left(\mu^* \frac{\partial v^*}{\partial y^*} \right) \frac{\mu_c}{\rho_c u_c x_c} \frac{x_c}{y_c} - \frac{2}{3} \frac{\partial}{\partial y^*} \left(\mu^* \frac{\partial u^*}{\partial x^*} \right) \frac{\mu_c}{\rho_c u_c x_c} \frac{x_c}{y_c}$$

$$+ \frac{\partial}{\partial x^*} \left(\mu^* \frac{\partial u^*}{\partial y^*} \right) \frac{\mu_c}{\rho_c u_c x_c} \frac{x_c}{y_c} + \frac{\partial}{\partial x^*} \left(\mu^* \frac{\partial v^*}{\partial x^*} \right) \frac{\mu_c}{\rho_c u_c x_c} \frac{y_c}{x_c}$$

All dimensionless variables in equations (18), (19), (20) and (21) are of order unity and the order of magnitude of each term is determined by its coefficient.

The value of K is determined by requiring that regions of overlaping validity exist between the sublayer and the boundary layer free interaction zone and between the latter and the inviscid outer flow. In the sublayer we require that the pressure and inertia terms be of the same order as the lowest order viscous terms. One can readily show that the coefficients of the terms $\frac{\partial}{\partial x}\left(u\frac{\partial u}{\partial x}\right)$, $\frac{\partial}{\partial x}\left(u\frac{\partial v}{\partial x}\right)$, $\frac{\partial}{\partial y}\left(u\frac{\partial v}{\partial x}\right)$ and $\frac{\partial}{\partial y}\left(u\frac{\partial u}{\partial y}\right)$ are higher order for $K>0$ and that to lowest order equation (18) simplies to

$$\rho^* u^* \frac{\partial u^*}{\partial x^*} + \rho^* v^* \frac{\partial u^*}{\partial y^*} = -\frac{\partial p^*}{\partial x^*} \tag{22}$$

$$+ \frac{\partial}{\partial y^*}\left(u^* \frac{\partial u^*}{\partial y^*}\right) \frac{\mu_c}{\rho_c u_c x_c} \frac{x_c^2}{y_c^2}$$

It follows from the above discussion and equation (22) that the viscous force in the sublayer will be of the same order of magnitude as the inertia forces and pressure force only if the characteristic parameter group $\frac{\mu_c}{\rho_c u_c x_c} \frac{x_c^2}{y_c^2}$ is of order unity. Thus, inserting the characteristic values given in equation (17) we require that

$$\frac{\mu_w}{\rho_w u_e R_e^{-k+\frac{1}{2}} \frac{I}{E}} \frac{\frac{L R_e^{k-1}}{\beta} \frac{E^2}{I}}{L^2 R_e^{-2k} I^2} = 1$$

which for a viscosity law which varies as T can be reduced to

$$\left(\frac{T_w}{T_e}\right)^2 \frac{E^3}{\beta I^4} R_e^{4k-\frac{5}{2}} = 1 \tag{23}$$

From equation (23) one observes that the only compatible value of K which allows the three forces to behave in a consistent manner is $K = 5/8$ and $I = \left(\frac{T_w}{T_e}\right)^{\frac{1}{2}} \frac{E^{\frac{1}{2}}}{\beta^{\frac{1}{2}}}$. Hence the thickness of the inner viscous sublayer is of $O(R_e^{-5/8})$ or $O(R_e^{-1/8}\,\delta)$. A related though different derivation is presented in Stewartson and Williams (1969). With $K = 5/8$ we may infer from equation (19) that $\frac{\partial p}{\partial y}$ is of the order $R_e^{-\frac{1}{4}}$. Thus, in the sublayer the equation of motion normal to the wall can be replaced to $O(R_e^{-\frac{1}{4}})$ by $\frac{\partial p}{\partial y} = 0$. Equations (20) and (21) can be simplified in the same manner. Inserting the value $K = 5/8$ in the reference quantities (15) one finds that in the free interaction zone the viscous terms in equation (20) are $O(R_e^{-\frac{1}{4}})$ less than the inertia and pressure terms and that in the y momentum equation (21) $\frac{\partial p}{\partial y}$ is of order $R_e^{-1/8}$. The momentum equation in the free interaction layer thus reduces to $O(R_e^{-\frac{1}{4}})$ to the same equation as for the inviscid flow in a quasi one dimensional stream tube. The dimensionless forms of the energy equation can be examined in a similar way. The essential results are as follows:

In the sublayer, we have

$$\rho u \frac{\partial h}{\partial x} + \rho v \frac{\partial h}{\partial y} = u \frac{dp}{dx} + \mu \left(\frac{\partial u}{\partial y}\right)^2 + \frac{\partial}{\partial y}\left(\frac{\mu}{P_r} \frac{\partial h}{\partial y}\right) \tag{24}$$

In the free interaction layer, the simplified form is

$$\rho u \frac{\partial h}{\partial x} + \rho v \frac{\partial h}{\partial y} = u \frac{dp}{dx} \tag{25}$$

2-2 Governing equations and boundary conditions

The order of magnitude non-dimensional analysis of the previous section gives the following essential results.

In the sublayer, the governing equations are

$$\frac{\partial}{\partial x}\rho u + \frac{\partial}{\partial y}\rho v = 0 \tag{26}$$

$$\rho u\frac{\partial u}{\partial x} + \rho v\frac{\partial u}{\partial y} = -\frac{dp}{dx} + \frac{\partial}{\partial y}\left(\mu\frac{\partial u}{\partial y}\right) \tag{27}$$

$$\rho u\frac{\partial h}{\partial x} + \rho v\frac{\partial h}{\partial y} = u\frac{dp}{dx} + \mu\left(\frac{\partial u}{\partial y}\right)^2 + \frac{\partial}{\partial y}\left(\frac{\mu}{Pr}\frac{\partial h}{\partial y}\right) \tag{28}$$

If the Prandtl number is assumed to be equal to 1, multiplying equation (27) by u and adding it to equation (28) gives

$$\rho u\frac{\partial H}{\partial x} + \rho v\frac{\partial H}{\partial y} = \frac{\partial}{\partial y}\left(\mu\frac{\partial H}{\partial y}\right) \tag{29}$$

where

$$H = h + \frac{u^2}{2} \tag{30}$$

Equations (26), (27) and (29) shall be solved in section 2-5 using integral methods. At the wall we shall require that the velocity profile satisfy the no slip condition and the two lowest order wall compatibility conditions that obtain from the equation of motion (27). Thus at y = 0,

$$u = 0 \quad , \quad \frac{\partial}{\partial y}\left(\mu\frac{\partial u}{\partial y}\right) = \frac{dp}{dx} \quad , \quad \frac{\partial^2}{\partial y^2}\left(\mu\frac{\partial u}{\partial y}\right) = 0 \tag{31}$$

Similarly, for the enthalpy profile we require at $y = 0$,

$$H = H_w \ , \qquad \frac{\partial}{\partial y}\left(\mu \frac{\partial H}{\partial y}\right) = 0 \tag{32}$$

In the free interaction layer, the governing equations are:

$$\frac{\partial}{\partial x}\rho u + \frac{\partial}{\partial y}\rho v = 0 \tag{33}$$

$$\rho u \frac{\partial u}{\partial x} + \rho v \frac{\partial u}{\partial y} = -\frac{dp}{dx} \tag{34}$$

$$\rho u \frac{\partial h}{\partial x} + \rho v \frac{\partial h}{\partial y} = u \frac{dp}{dx} \tag{35}$$

or in terms of the stagnation enthalpy H,

$$\rho u \frac{\partial H}{\partial x} + \rho v \frac{\partial H}{\partial y} = 0 \tag{36}$$

At the boundary layer edge $y = \delta$, we require the inviscid outer flow to be adiabatic.

$$H = H_e \tag{37}$$

The junction of the inner viscous sublayer and outer free interaction layer is at the sublayer edge $y = \epsilon$. Here we require that the profiles match continuously in both value and slope with the profile descriptions in the free interaction layer denoted by subscript ϵ. Therefore, the matching conditions are:
at $y = \epsilon$,

$$\begin{aligned} u = u_\epsilon \ , \ \frac{\partial u}{\partial y} = \left(\frac{\partial u}{\partial y}\right)_{at\, y=\epsilon} \ , \ \psi = \psi_\epsilon \\ H = H_\epsilon \ , \ \frac{\partial H}{\partial y} = \left(\frac{\partial H}{\partial y}\right)_{at\, y=\epsilon} \end{aligned} \tag{38}$$

2-3 Derivation of the basic interaction relation

In this section, the basic interaction equation relating the flow inclination at $y = \epsilon$ and $y = \delta$ is derived. For the sake of readability and completeness the details of the derivation are presented. The governing equations for the free interaction zone (33), (34), (35) and the equation of state are repeated below

$$\frac{\partial}{\partial x}\rho u + \frac{\partial}{\partial y}\rho v = 0 \tag{39}$$

$$\rho u \frac{\partial u}{\partial x} + \rho v \frac{\partial u}{\partial y} = -\frac{dp}{dx} \tag{40}$$

$$\rho u \frac{\partial h}{\partial x} + \rho v \frac{\partial h}{\partial y} = u \frac{dp}{dx} \tag{41}$$

$$p = \frac{\gamma - 1}{\gamma} \rho h \tag{42}$$

Eliminating $\frac{\partial \rho}{\partial x}$ and $\frac{\partial \rho}{\partial y}$ through equation (42), one can rewrite equation (39) as

$$\rho \frac{\partial u}{\partial x} + \frac{\gamma}{\gamma - 1} \frac{u}{h} \frac{dp}{dx} - \frac{\rho u}{h} \frac{\partial h}{\partial x} + \rho \frac{\partial v}{\partial y} - \frac{\rho v}{h} \frac{\partial h}{\partial y} = 0 \tag{43}$$

or

$$\rho \frac{\partial u}{\partial x} + \rho \frac{\partial v}{\partial y} + \frac{\gamma}{\gamma - 1} \frac{u}{h} \frac{dp}{dx} - \frac{1}{h}\left(\rho u \frac{\partial h}{\partial x} + \rho v \frac{\partial h}{\partial y}\right) = 0 \tag{44}$$

The convenient x-derivative is $\frac{d P}{d x}$, since only this x-derivative is constant across the viscous layer and can be removed from under the integral sign in an integration in the y direction. This is important since the key

relation in the interaction process is the integral of equation (39) taken across the inviscidly behaving portion of the boundary layer. Now eliminating $\frac{\partial u}{\partial x}$, $\frac{\partial h}{\partial y}$ and $\frac{\partial h}{\partial y}$ in equation (44) in favor of $\frac{dP}{dx}$ through the use of the equations (40) and (41), one finds after some rearrangement

$$\frac{u\frac{\partial u}{\partial y} - v\frac{\partial u}{\partial y}}{u^2} = \frac{1}{\rho u^2}\frac{dp}{dx} + \frac{1}{\rho h}\frac{dp}{dx} - \frac{1}{\rho h}\frac{\gamma}{\gamma-1}\frac{dp}{dx} \qquad (45)$$

or

$$\frac{\partial}{\partial y}\left(\frac{v}{u}\right) = -\frac{1}{\gamma p}\frac{dp}{dx}\frac{M^2-1}{M^2}, \quad 0 \le y \le \delta \qquad (46)$$

where

$$M^2 = \frac{u^2}{(\gamma - 1)\, h} \qquad (47)$$

This equation (46) is essentially a pressure-area relation for a fluid streamtube of differential thickness dy . One notes that it simply shows the relation between the adiabatic expansion of the streamtube area and the pressure gradient in the x-direction. This behavior is directly equivalent to inviscid quasi one-dimensional stream tube flow. (see equation (2.1) from Weinbaum and Garvine (1969))

$$\frac{1}{A}\frac{dA}{dx} = -\frac{1}{\gamma p}\frac{dp}{dx}\frac{M^2-1}{M^2} \qquad (48)$$

Integrating equation (46) from $y = \epsilon$ to $y = \delta$, one obtains

$$\tan\theta_e - \tan\theta_\epsilon = -\frac{1}{\gamma p}\frac{dp}{dx}\int_\epsilon^\delta \frac{M^2-1}{M^2}\, dy \qquad (49)$$

The integral equation (49) differs from the corresponding result equation (3.9) in Weinbaum and Garvine (1969)

$$\tan\theta_e = \int_0^\delta \frac{M^2-1}{M^2}\, dy \qquad (50)^{***}$$

(equation (50) is not applicable to a body boundary layer, since M vanishes at the wall and the integral is singular)***

for a free shear layer because of the non-vanishing lower limit ϵ on the integral and the fact that the u and h profiles in the expression for M can not be specified arbitrarily but must obey wall compatibility conditions involving the local streamwise pressure gradient and the local wall heat transfer.

Equation (49) is the basic interaction equation coupling the three flow regions. θ_e, the local flow angle at the boundary layer edge, is determined by the local Mach number at the edge of the boundary layer through the use of Prandtl-Meyer relation for the outer flow which is assumed to be a simple outgoing wave system comprised of isentropic compression and expansion waves generated by the combined displacement interaction of the sublayer and free interaction layer. Using the standard definition of the Prandtl-Meyer function (M)

$$\theta(x) = \nu(M_\infty) - \nu(M_e) - \theta_w(x) \qquad (51)$$

where $\theta_w(x)$ is the inclination of the local wall tangent to the horizontal surface. θ_ϵ , the local streamline angle at the edge of sublayer, describes the displacement effect of the inner viscous region. The integral term on the right hand side represents the integrated streamtube pressure-area relation for the free interaction zone, This is an inviscid rotational flow with no normal pressure gradient as discussed previously.

2-4 Solution of the equations for inviscid interaction layer

The approximation introduced by equations (33), (34) and (35) greatly simplifies the solution for u , h and M in the inviscid interaction layer. One need not resort to a costly method of characteristics calculation to describe the wave interaction effects that occur in this layer but can represent the layer instead by a continuous distribution of rotational inviscid streamtubes. Since both the entropy S and the stagnation enthalpy H are conserved along each streamtube, one is thus led to the use of Von Mises coordinates x , ψ as the natural choice of coordinates for the free interaction layer. Transforming equation (49) into Von Mises coordinates one obtains (the detailed derivation is shown in appendix C)

$$\tan\theta_e - \tan\theta_\epsilon = -\frac{1}{\gamma p^2}\frac{dp}{dx}\frac{P_\infty}{T_\infty}\frac{1}{(\gamma R)^{\frac{1}{2}}}\int_{\psi_\epsilon}^{\psi_s}\frac{M^2-1}{M^3(\psi,x)}T^{\frac{1}{2}}(\psi,x)\,d\psi \qquad (52)$$

The Mach number variation $M(\psi, x)$ along a streamline ψ is obtained directly from the inviscid streamtube relations.

$$M(\psi,x) = \left(\frac{2}{\gamma-1}\right)^{\frac{1}{2}}\left[\left(\frac{P(x)}{P_1}\right)^{\frac{1-\gamma}{\gamma}}\left(1+\frac{\gamma-1}{2}M_1^2(\psi)\right)-1\right]^{\frac{1}{2}} \qquad (53)$$

where P_1 and $M_1(\psi)$ are known initial conditions at the start of the interaction and $P(x)$ is the local interaction pressure at the edge of the boundary layer. Similarly the temperature profile $T(\psi)$ is readily related to $M(\psi, x)$ given by equation (53) through the algebraic adiabatic streamtube relation for a perfect gas.

$$T(\psi, x) = T_1(\psi) \frac{1 + \frac{\gamma-1}{2} M_1^2(\psi)}{1 + \frac{\gamma-1}{2} M^2(\psi, x)} \tag{54}$$

While the velocity profile $u(\psi, x)$ is obtained from equations (47), (53) and (54)

$$\frac{u(\psi, x)}{u_e(\psi, x)} = \frac{T(\psi, x)^{\frac{1}{2}}}{T_e(x)^{\frac{1}{2}}} \frac{M(\psi, x)}{M_e(x)} \tag{55}$$

2-5 The treatment of the inner viscous sublayer

The establishment of the sublayer edge ϵ and the determination of the local displacement angle θ_ϵ of the sublayer are both the most critical and subtle elements of the present theory. The order of magnitude analysis presented in section 2-1 shows that the ratio of the sublayer to boundary layer thickness is proportional to

$$\frac{\epsilon}{\delta} \propto \frac{\left(1+\frac{\gamma-1}{2}M_e^2\right)^{\frac{1}{2}} Re^{-\frac{1}{8}}}{\left(M_e^2-1\right)^{\frac{1}{8}} E^{\frac{1}{4}}} \qquad (56)$$

$$E = \sqrt{2}\int_0^{2\delta} \frac{T}{T_e}\, d\eta$$

where η is a dimensionless boundary layer coordinate which is of order unity. The factor multiplying $R_e^{-1/8}$ takes on values which typically lie in the range from 1 to 3 for $M \leq 10$. Since the exact value of the proportionality constant is not known it is conceivable that for a laminar boundary layer in the range $10^4 \leq R_e \leq 10^6$ the viscous sublayer might occupy a significant portion of the entire boundary layer. The numerical experiments which will be discussed in section 2-8 show that representative values of the ratio of $\frac{\epsilon_1}{\delta_1}$ lie in the range of 0.4 to 0.7 for adiabatic laminar boundary layers. Thus, one concludes that for laminar flow the sublayer can not be treated as a thin incompressible boundary layer as originally proposed by Lighthill and assumed by Stewartson and Williams. Yet, the inviscidly behaving layer is sufficiently large for shock reflection and wave interference effects to be important at high Mach numbers.

The description of the sublayer is complicated by two factors: (1) the importance of compressibility effects due to the unexpectedly large thickness of the sublayer so the flow here behaves like a compressible fluid in which the conventional compressible boundary layer equations apply and (2) the fact that the velocity and temperature gradients do not vanish at the edge of the sublayer as they do at the edge of the boundary layer in ordinary boundary layer theory. The first of these complications is readily handled through the standard technique of first transforming the compressible boundary layer equations into their incompressible form by using a modified Stewartson transformation such as that employed by Cohen and Reshotko (1956).

$$dX = \lambda \frac{a_e P_e}{a_\infty P_\infty} dx \quad , \quad dY = \frac{a_e \rho}{a_\infty \rho_\infty} dy$$

$$U = \frac{\partial \psi}{\partial Y} \quad , \quad V = \frac{\partial \psi}{\partial X} \tag{57}$$

Assuming a linear viscosity law

$$\frac{\mu}{\mu_\infty} = \lambda \frac{T}{T_\infty} \tag{58}$$

and applying equations (57) and (58) to the boundary layer equations (26) and (27), one obtains the following transformed equations (the analogs of the incompressible form of the compressible boundary layer equations):

$$\frac{\partial U}{\partial X} + \frac{\partial V}{\partial Y} = 0 \tag{59}$$

$$U \frac{\partial U}{\partial X} + V \frac{\partial U}{\partial Y} = U_e \frac{dU_e}{dX}(1+S) + \nu_\infty \frac{\partial^2 U}{\partial Y^2} \tag{60}$$

where the enthalpy function S is defined for convenience as

$$S = \frac{H}{H_e} - 1 \tag{61}$$

The second complication is treated by deriving a new momentum integral equation from (59) and (60) and imposing novel boundary conditions on the sublayer profiles at their outer edge. The detailed derivation which is shown in appendix D leads to the following result:

$$\frac{\partial \theta^*}{\partial X} - \frac{\theta^* dU_E}{U_E dX}\left(2 + \frac{\delta^*}{\theta^*} - \frac{E}{\theta^*} - \frac{U_e}{U_E}\frac{\frac{dU_e}{dX}}{\frac{dU_E}{dX}}\frac{1}{\theta^*}\int_0^E (1+S)\,dY\right)$$

$$- \frac{\nu_{0\infty}}{U_E^2}\frac{\tau_E}{\mu_E} + \frac{\nu_{0\infty}}{U_E^2}\frac{\tau_W}{\mu_W} = 0 \qquad (62)$$

where

$$\theta^* = \int_0^E \frac{U}{U_E}\left(1 - \frac{U}{U_E}\right) dY$$

$$\delta^* = \int_0^E \left(1 - \frac{U}{U_E}\right) dY$$

As one might anticipate the new terms in the momentum integral equation come from the non-vanishing shear stress τ_E at the sublayer edge Y = E and the fact that conditions at Y = E (the transformed sublayer edge) and Y = Δ (the transformed boundary layer edge) differ. The transformed boundary conditions on the velocity and stagnation enthalpy profiles at the wall Y = 0 obtained from equations (31) and (32) are the same as in ordinary boundary layer theory. They are expressed as follows (see appendix D)

$$U = 0 \quad , \quad \frac{\partial^2 U}{\partial Y^2} = \frac{\frac{dp}{dx}}{\mu_{0\infty}\left(\frac{T_e}{T_{0\infty}}\right)^{\frac{3}{2}}\frac{p}{p_{0\infty}}\frac{\rho_W}{\rho_{0\infty}}}$$

$$\frac{\partial^3 U}{\partial Y^3} - \frac{1}{T_W}\frac{\partial T}{\partial Y}\frac{\partial^2 U}{\partial Y^2} = 0 \qquad (63)$$

$$S = S_W \quad , \quad \frac{\partial^2 S}{\partial Y^2} = 0$$

At Y = E (the transformed sublayer edge) we require that the profiles match continuously in both value and slope with the profile descriptions in the free interaction layer denoted by subscript E. From equation (38)

$$U = U_E \quad , \quad \frac{\partial U}{\partial Y} = \left(\frac{\partial U}{\partial Y}\right)_E \quad , \quad \psi = \psi_E \tag{64}$$

$$S = S_E \quad , \quad \frac{\partial S}{\partial Y} = \left(\frac{\partial S}{\partial Y}\right)_E \tag{65}$$

The new profiles thus differ from the usual Karman-Pohlhausen profiles for the boundary layer flow in the appearence of velocity and stagnation enthalpy gradient terms at the sublayer edge.

Introducing a dimensionless coordinate $\xi = \frac{Y}{E}$ the sublayer profiles can be expressed as follows:
(the detailed derivation is shown in appendix E)

$$\frac{U}{U_E} = A\xi + B\xi^2 + C\xi^3 + D\xi^4 \tag{66}$$

$$S = \bar{A}\xi + \bar{B}\xi^2 + \bar{C}\xi^3 + \bar{D}\xi^4 \tag{67}$$

$$\Lambda = \frac{\frac{dp}{dx}}{\mu_{o\infty}\frac{U_E}{E^2}\left(\frac{T_e}{T_{o\infty}}\right)^{\frac{3}{2}}\frac{P}{P_{o\infty}}\frac{\rho_w}{\rho_{o\infty}}} \tag{68}$$

$$A = \frac{4}{3} - \frac{2}{3}B - \frac{1}{3}C - \frac{1}{3}\frac{\partial\left(\frac{U}{U_E}\right)}{\partial\xi} \text{ at } \xi = 1$$

$$B = -\frac{\Lambda}{2}$$

$$C = -\frac{\Lambda}{6}\frac{B}{1+S_w} \tag{69}$$

$$D = -\frac{1}{3} - \frac{B}{3} - \frac{2}{3}C + \frac{1}{3}\frac{\partial\left(\frac{U}{U_E}\right)}{\partial\xi} \text{ at } \xi = 1$$

$$\bar{A} = S_w$$

$$\bar{B} = \frac{3}{2}S_{\text{at }\xi=1} - \frac{3}{2}S_w - \frac{1}{2}\frac{\partial S}{\partial\xi} \text{ at } \xi = 1$$

$$\bar{C} = 0 \tag{70}$$

$$\bar{D} = \frac{1}{2}S_w - \frac{1}{2}S_{\text{at }\xi=1} + \frac{1}{2}\frac{\partial S}{\partial\xi} \text{ at } \xi = 1$$

The matching condition $\psi = \psi_\epsilon$ in equation (64) at the sublayer edge is automatically satisfied since the derivation of the sublayer momentum integral equation (62) already contains an integral form of the continuity equation. At the sublayer edge $\xi = 1$, the ξ derivatives in equations (69) and (70) can be expressed in terms of ψ derivatives obtained from the inviscid layer solutions (53), (54) and (55).

$$\frac{\partial\left(\frac{u}{u_\epsilon}\right)}{\partial \xi \text{ at } \xi=1} = \frac{\partial\left(\frac{u}{u_\epsilon}\right)}{\partial\left(\frac{\psi}{u_\infty \delta_1}\right) \text{ at } \psi_\epsilon} \left(1+\frac{\gamma-1}{2}M_\infty^2\right)^{\frac{1}{2}} \frac{\epsilon}{\delta_1} \frac{M_e}{M_\infty} \tag{71}$$

$$\frac{\partial S}{\partial \xi \text{ at } \xi=1} = \frac{\partial S}{\partial(\psi/u_\infty \delta_1) \text{ at } \psi_\epsilon} \left(1+\frac{\gamma-1}{2}M_\infty^2\right)^{\frac{1}{2}} \frac{\epsilon}{\delta_1} \frac{M_e}{M_\infty} \tag{72}$$

One more comment can be added here. The basic equation (52) for the interaction pressure is fundamentally different from the related equation that obtains from the integral method in the single layer theories where the local wall pressure gradient is uncoupled from the velocity profiles. The latter is a first order differential equation for P whereas in the present theory the differential equation for P is second order. This is readily seen by integrating the continuity equation across the sublayer and evaluating $\tan\theta_\epsilon$. This expression is (the derivation is shown in appendix F)

$$\tan\theta_\epsilon = \frac{\epsilon \int_0^1 \frac{\partial(\rho u)}{\partial x} \frac{\rho_\infty}{\rho} d\xi}{\rho_\epsilon u_\epsilon \left(\frac{a_e}{a_\infty}\right)^2} \tag{73}$$

where from the velocity profile (66) the X derivative in the integral introduces terms in $\frac{d^2P}{dx^2}$. In contrast to the existing single layer theories, both P and $\frac{dP}{dx}$ must be spedified at the initial station in triggering the pressure interaction.

2-6 The initial conditions

One can proceed with the numerical integration of equation (52) for a typical viscid-inviscid interaction problem only if the velocity and enthalpy profiles can be prescribed at the onset of the interaction. In the problems considered in this investigation it is assumed that the flow upstream of the strong pressure interaction is that for a thin flat plate immersed at zero incidence in a uniform stream of u_∞. Viscous forces at the wall form a boundary layer downstream of the leading edge while the flow upstream of the leading edge is not affected. The plate wall is maintained at a constant temperature T_w. The calculation of the flow field in region of interaction is started at a distance x_1 from the leading edge where the boundary layer is assumed to be fully developed. The viscid-inviscid interaction is caused either by an externally generated oblique shock incident on the wall or by a forward facing edge corner far downstream. The velocity profile at position x_1 is determined by the standard Blasius solution where distortions of the velocity profile due to interaction are small and can be neglected.

The Blasius equation is

$$f'''(\zeta) + ff'' = 0 \tag{74}$$

with boundary conditions

$$\begin{aligned} f(0) &= f'(0) = 0 \\ \lim f'(\zeta) &= 1 \quad \text{as } \zeta \to \infty \end{aligned} \tag{75}$$

The velocity components are represented as

$$\begin{aligned} u &= u_\infty f'(\zeta) \\ v &= \left(\frac{1}{2}\frac{\nu u_\infty}{x}\right)^{\frac{1}{2}} (\zeta f'(\zeta) - f(\zeta)) \end{aligned} \tag{76}$$

The analytic solution of the equation (74) can not be given in closed form and must be gotten numerically. H. Blasius obtained the solution in the form of a power series expansion about $\zeta = 0$ and an asymptotic expansion for $\zeta_\delta = \infty$. (Here we use the value $\zeta_\delta = 3.8$, or $\frac{u}{u_\infty} = 0.995944$ as the boundary layer outer edge). The two solutions are joined at a suitable point (we pick $\zeta_{joint} = 2.6$). The power series expansion for $f(\zeta)$ near $\zeta = 0$ was calculated by H. Blasius

$$f(\zeta) = \sum_0^\infty (-1)^n C_n \zeta^{3n+2} \tag{77}$$

where

$$f''(0) = 0.4696 \tag{78}$$

$C_0 = \frac{1}{2} f''(0)$ $\qquad$ $C_3 = (375/11!)\,(2C_0)^4$

$C_1 = (1/5!)\,(2C_0)^2$ $\qquad$ $C_4 = (27897/14!)\,(2C_0)^5$

$C_2 = (11/8!)\,(2C_0)^3$ $\qquad$ $C_5 = (3817137/17!)\,(2C_0)^6$

The asymptotic solution for large value of ζ is as follows:

$$f(\bar{\zeta}) = \bar{\zeta} - \beta + \gamma \int_\infty^{\bar{\zeta}} d\bar{\zeta} \int_\infty^{\bar{\zeta}} \exp\left[-\tfrac{1}{4}(\bar{\zeta}-\beta)^2\right] d\bar{\zeta} \tag{79}$$

where

$$\bar{\zeta} = \sqrt{2}\,\zeta$$

$$\alpha = 0.332 \tag{80}$$

$$\beta = 1.73$$

$$\gamma = 0.231$$

The solution of equation (74) is tabulated in many texts.

As mentioned previously both P and $\frac{dp}{dx}$ at the initial station must be specified in order to start the pressure interaction. The series expansion solution for a self-induced weak pressure interaction at high Mach numbers is given in Lees and Probstein (1959), and has been found to agree satisfactory with experimental results (Kendall, J. M., Jr., 1957 and Bertram, M. H., 1957)

The fundamental interaction parameter $\tilde{X}$ is defined as

$$\tilde{X} = \frac{M_\infty^3}{R_{e\infty}^{\frac{1}{2}}} \tag{81}$$

and the weak interaction induced pressure on an insulated flat plate in air (r = 1.4) is

$$\frac{P}{P_\infty} = 1.0 + 0.335\,\tilde{X} + 0.0481\,\tilde{X}^2 \tag{82}$$

In the case of flow with heat transfer the weak interaction induced pressure is

$$\frac{P}{P_\infty} = 1.0 + r\,d_{orig}\,\tilde{X} + \frac{r\,(\,r+1\,)}{4}\,d_{orig}^{\,2}\,\tilde{X}^2 \tag{83}$$

The initial value for $\frac{dp}{dx}$ can be readily obtained by differentiating the above equations with respect to x . The basic parameters that have to be specified for a typical interaction problem are M_∞ , $R_{e\infty}$ and S_w . The fundamental interaction parameter $\tilde{X}$ and the weak interaction induced pressure can be determined easily from equations (81) and (82).

The initial edge Mach number is obtained from

$$M_{e_1} = \left(\frac{2}{r-1}\right)^{\frac{1}{2}} \left(\frac{1 + \frac{r-1}{2} M_\infty^2}{(P_1/P_\infty)^{\frac{r-1}{r}}} \right)^{\frac{1}{2}} \tag{84}$$

The various flow variables at the initial station 1 can be found in terms of η by the following functional relations:

The temperature and enthalpy function profiles are represented respectively by

$$\frac{T}{T_e} = \left(1 + \frac{r-1}{2} M_e^2 \right) (1+S_w) - \frac{r-1}{2} M_e^2\, f'(\eta)^2 \tag{85}$$

$$S = \left(1 - \frac{U}{U_e} \right) S_w \tag{86}$$

S_w is the enthalpy function evaluated at the wall which determines the wall temperature through the relation

$$T_w = T_o\,(1 + S_w) \tag{87}$$

Thus, $S_w = 1$ corresponds to a wall temperature of absolute zero, $S_w = 1$ to a wall at twice the free stream stagnation temperature and $S_w = 0$ to a wall at the free stream stagnation temperature which for $P_r = 1$ represents an insulated surface.

The Mach number profile is related to ζ by

$$M_1 = M_{e_1} \frac{\left(\frac{u}{u_e}\right)_1}{\left(\frac{T}{T_e}\right)_1^{\frac{1}{2}}} \tag{88}$$

The dimensionless normal coordinate $\frac{y}{\delta_1}$, the dimensionless transformed normal coordinate $\frac{Y}{\delta_1}$, and the dimensionless stream function $\frac{\psi}{u_\infty \delta_1}$ are related to ζ by the following expressions

$$y_1^* = \frac{y_1}{\delta_1} = \frac{\left(\int_0^{\zeta} \frac{T}{T_e} d\zeta\right)_1}{\left(\int_0^{\zeta_\delta} \frac{T}{T_e} d\zeta\right)_1} \tag{89}$$

$$Y_1^* = \frac{Y_1}{\delta_1} = \frac{\zeta_1 \left(\frac{P_1}{P_\infty}\right)^{\frac{n+1}{2n}}}{\left(\int_0^{\zeta_\delta} \frac{T}{T_e} d\zeta\right)_1 \left(1 + \frac{n+1}{2} M_\infty^2\right)^{\frac{(n+1)}{(n-1)2}}} \tag{90}$$

$$\psi_1^* = \frac{\psi}{u_\infty \delta_1} = \frac{f(\zeta)_1 \frac{M_{e_1}}{M_\infty} \left(\frac{P_1}{P_\infty}\right)^{\frac{n+1}{2n}}}{\left(\int_0^{\zeta_\delta} \frac{T}{T_e} d\zeta\right)_1 \left(1 + \frac{n+1}{2} M_\infty^2\right)^{\frac{1}{n-1}}} \tag{91}$$

If the initial sublayer thickness $\epsilon_1^* = \frac{\epsilon_1}{\delta_1}$ is determined, ζ_ϵ can be found implicitly from the functional relationship between y and ζ, Cohen and Reshotko (1956)

$$y = \frac{\rho_\infty}{\rho_e} \frac{a_\infty}{a_e} \left(\frac{2 \nu_\infty x}{u_e}\right)^{\frac{1}{2}} \int_0^{\zeta} \frac{T}{T_e} d\zeta \tag{92}$$

Consequently, the initial values and slopes (i.e. the matching conditions) for all the flow variables at the sublayer edge can be determined in a straight forward manner

$$\left(\frac{d\left(\frac{\psi}{u_\infty \delta_1}\right)}{d\zeta}\right)_1 = \frac{(f'(\zeta))_1}{\left(\int_0^{\zeta_1} \frac{\rho}{\rho_e} d\zeta\right)_1} \frac{\left(\frac{M_{e_1}}{M_\infty}\right)\left(\frac{p_{e_1}}{p_\infty}\right)^{\frac{\gamma+1}{2\gamma}}}{\left(1+\frac{\gamma+1}{2} M_\infty^2\right)^{\frac{1}{\gamma-1}}}$$

$$\left(\frac{d\left(\frac{u}{u_e}\right)}{d\left(\frac{\psi}{u_\infty \delta_1}\right)}\right)_1 = \frac{(f''(\zeta))_1}{\left(\frac{d\left(\frac{\psi}{u_\infty \delta_1}\right)}{d\zeta}\right)_1}$$

$$\left(\frac{d\left(\frac{T}{T_e}\right)}{d\left(\frac{\psi}{u_\infty \delta_1}\right)}\right)_1 = \frac{\left(-(\gamma-1) M_{e_1}^2 \left(\frac{u}{u_e}\right) f''(\zeta)\right)_1}{\left(\frac{d\left(\frac{\psi}{u_\infty \delta_1}\right)}{d\zeta}\right)_1}$$

$$\left(\frac{dM}{d\left(\frac{\psi}{u_\infty \delta_1}\right)}\right)_1 = \frac{\left(M_e \frac{f''(\zeta)}{T/T_e} - \frac{1}{2} M_e \frac{u}{u_e} \frac{(\gamma-1) M_e^2 \frac{u}{u_e} f''(\zeta)}{(T/T_e)^{3/2}}\right)_1}{\left(\frac{d\left(\psi/u_\infty \delta_1\right)}{d\zeta}\right)_1}$$

These relations together with the wall compatibility conditions and the boundary conditions determine the sublayer velocity and enthalpy profiles described by the polynomial approximations (66) and (67). In the free interaction zone an interpolation method is used to express all flow quantities in terms of the stream function ψ instead of ζ . This completes the description of the initial conditions required to trigger the self-sustaining viscid-inviscid boundary layer flow interaction.

2-7 The cyclic process of determining the continuous interaction

The calculation is initiated at a distance x_1 from the flat plate leading edge. Initial values for the pressure and the pressure gradient at x_1 are obtained from the weak interaction induced pressure equations (82) or (83). The initial value of $\frac{\epsilon_1}{\delta_1}$ is not known and has to be determined by the trial and error forward integration procedure described in the next section. However, having assumed some initial value for $\frac{\epsilon_1}{\delta_1}$ the initial profiles of u, T, M and the sublayer edge matching conditions can be determined as a function of ξ and ψ as described in the previous section.

The edge value of the streamline inclination angle is related to the edge Mach number through the Prandtl-Meyer relation (51) with $\theta_w = 0$. The transformed sublayer momentum thickness θ^* is evaluated for the profile (66) and is readily shown to be of the form (see derivation in appendix G)

$$\theta^* = \epsilon \left(\alpha_1 + \alpha_2 \Lambda + \alpha_3 \Lambda^2 \right) \qquad (93)$$

where the coefficients α_i depend on S_w and the sublayer edge conditions.

$\left(\frac{\partial \theta^*}{\partial x}\right)_1$ is then determined from equation (62) using the initial value of θ^* determined from (93). The evaluation of θ_{ϵ_1} is accomplished by applying the free interaction equation (52).

A forward difference approximation is used to find the boundary layer and sublayer edge thickness at the next station

$$\frac{\delta_2}{\delta_1} = \frac{\delta_1}{\delta_1} + \tan\theta_{e_1} \frac{\Delta x}{\delta_1} \tag{94}$$

$$\frac{\epsilon_2}{\delta_1} = \frac{\epsilon_1}{\delta_1} + \tan\theta_{\epsilon_1} \frac{\Delta x}{\delta_1} \tag{95}$$

similarly,

$$\frac{p_2}{p_\infty} = \frac{p_1}{p_\infty} + \left(\frac{d\left(\frac{p}{p_\infty}\right)}{d\left(\frac{x}{\delta_1}\right)}\right)_1 \frac{\Delta x}{\delta_1} \tag{96}$$

$$\theta_2^* = \theta_1^* + \left(\frac{d\theta^*}{d(x/\delta_1)}\right)_1 \frac{\Delta x}{\delta_1} \tag{97}$$

where Δ x is the step size in the forward integration.

At station 2, all the other flow properties, except $\left(\frac{dp}{dx}\right)_2$ and $\theta_{\epsilon 2}$, are related to the static pressure P_2 and are therefore determined. The matching conditions are also related to P_2. Since the various coefficients in the profile relations (66) through (70) are functions of x the evaluation of $\tan\theta_\epsilon$ in (73) is extremely tedious and an alternate but entirely equivalent procedure is used.

The value of θ^* obtained from (97) is inserted into (93) and the latter solved for the profile parameter Λ at the station 2. The quadratic equation for Λ has only one physically meaningful root and this root is used to determine the new value of $\frac{dp}{dx}$ using the definition of Λ following equation (68). The interaction equation (52) then provides the new value of the streamline inclination angle θ_ϵ at the sublayer edge. All the unknown flow parameters at station 2 have now been determined and the calculation can proceed to the next station where the same procedure is repeated.

2-8 The determination of the sublayer edge

The selection of the sublayer edge is a rather subtle task since in the case of laminar boundary layer interaction the R_e is not large enough for the sublayer to be a small portion of the total boundary layer as required in the asymptotic analysis of Stewartson and Williams. One might perform numerical experiments of the type described by Rose (1970) to get a qualitative idea of where in the velocity profile the disturbances due to the interaction pressure field are no longer significantly affected by viscous stresses. This procedure while ad hoc is somewhat satisfactory for turbulent boundary layers where there is an abrupt change in velocity gradient as one proceeds from the laminar sublayer into the buffer layer. In actuality, a well defined criterion for choosing the effective sublayer edge does exist because of the unique characteristic of the interaction pressure field that the pressure required to separate a specified boundary layer profile is independent of the downstream disturbance.

Both existing theories and experiments indicate that the incipient pressure at separation depends only on M_∞, $R_{e\infty}$ and the S_w at the start of the interaction.

Since P at separation in the present model depends on the definition of ϵ, one anticipates that as the guessed value of the ratio of the sublayer to boundary layer thickness at the initial station $\frac{\epsilon_1}{\delta_1}$ is increased, one should eventually reach a value of $\frac{\epsilon_1}{\delta_1}$ where further increases should not produce significant changes in the predicted value of the incipient separation pressure as

determined by a downstream integration, provided an effective sublayer edge does exist. Furthermore, for this value of $\frac{\epsilon_1}{\delta_1}$ the predicted value of P at separation should agree with experiment.

The numerical experiments just described have been performed and clearly demonstrate the validity of this basic hypothesis. The results of a typical set of experiments for a prescribed boundary layer profile are shown in figure 4. It is seen that the separation pressure becomes insensitive to $\frac{\epsilon_1}{\delta_1}$ and that a gradual maximum is achieved wherein further increases in $\frac{\epsilon_1}{\delta_1}$ only lead to a slight decrease in separation pressure due to the inclusion of too much of the inviscid interaction flow in the viscous sublayer. All values of $\frac{\epsilon_1}{\delta_1}$ in the range $0.22 \leq \frac{\epsilon_1}{\delta_1} \leq 0.48$ predict the separation pressure and the entire pressure profile up to separation to within a few percent for the particular $M_\infty = 2$ flow configuration considered. It is convenient to choose $\frac{\epsilon_1}{\delta_1}$ corresponding to the maximum in the curve. The excellent agreement between theory and experiment for this value of $\frac{\epsilon_1}{\delta_1}$ is evident from figure 8 where the growth of the interaction pressure field through the point of separation is shown.

2-9 The treatment of flow region in the immediate vicinity of shock impingement

The flow region in the immediate vicinity of shock impingement, the region between stations A and B in figure 1, requires special treatment because of the important shock impingement effects that result locally from the reflection of the incident shock wave. It is commonly thought that the incident shock must be locally reflected at the sonic line as an expansion fan of equal strength if the viscous sublayer is not to experience a sudden pressure rise. Previous investigators could not reconcile this behavior with the fact that large normal pressure gradients must be generated as the shock propagates through the supersonic portion of the boundary layer. This behavior did not appear consistent with the experimental observation and the theoretical prediction of the asymptotic theory for large R_e that the normal pressure gradients upstream of station A and downstream of station B are small. The vanishing of the normal pressure gradients can be explained if the refraction of the incident oblique shock by the Mach number profile of the boundary layer is balanced by an equal strength but opposite reflected expansion fan.

To relate conditions at stations A and B , we assume that on the length scale of the complete interaction the region A-B can be viewed as a discontinuity in which the combined turning angle of the incident oblique shock wave and the reflected expansion fan vary smoothly across the inviscid interaction layer. The velocity profile , enthalpy profile and Mach number profile do not change on this length scale and the static pressure is continuous. The streamline

angles θ_e and θ_ϵ, however, are discontinuous because the flow streamlines at the boundary layer and sublayer edge are turned by both the incident oblique shock and the reflected expansion fan. For a given shock strength, values of $\Delta\theta_e$ and $\Delta\theta_\epsilon$ are readily determined using the oblique shock and Prandtl-Meyer wave relations.

The same mathematical model used to describe the interaction up to the location of shock impingement, station A, can be continued downstream of station B. No difficulty is encountered in integrating equations (52) and (62) through the reattachment point, this local region is similar in structure to the local region about the separation point.

In the case of wedge-induced interaction the velocity profile, enthalpy profile and wall pressure are considered to be continuous at the wedge corner. However, the flow at boundary layer edge, is deflected away from the wall through an angle equal to the wedge angle. For a given wedge angle, all conditions immediately downstream of the wedge corner are uniquely determined and the downstream integration can be performed without difficulty.

3 Numerical results and discussions

Numerical calculations have been carried out for a variety of adiabatic and non-adiabatic laminar boundary layer interactions at supersonic speeds. Comparisons of the numerical results with previous experimental measurements are shown where such data are available.

3-1 The nature of solution of the interaction equation

It is well known from earlier studies, for example, Garvine (1968), Baum (1966), Stewartson (1969) and Klineberg and Lees (1969), that the solutions to the interacting boundary layer equations exhibit a saddle point type behavior with respect to the initial value assumed for the interaction pressure or Mach number at the start of the interaction. Two types of downstream flow behavior are observed: (1) the interacting boundary layer generates its own adverse pressure gradient downstream and eventually separates from the wall, (2) it generates a favorable pressure gradient downstream and the flow accelerates without bound. Between these two sets of diverging solutions there exists an appropriate value of the initial interaction pressure or Mach number which gives the neutrally stable solution. In the present analysis, the static pressure has been selected as the perturbation parameter to start the self-sustaining boundary layer interaction.

Figure 3 shows the effect of varying the initial starting pressure for the interaction (i.e. the dependence of the solution on the initial perturbation parameter). Small changes in the initial value of the interaction pressure cause large variations in downstream behavior. Garvine (1968) has shown that this behavior arises because the boundary value problem for self induced interaction is not well posed as an initial value problem. The boundary condition imposed by the displacement interaction contains elliptic features due to the presence of double streamwise derivatives which appear in the integral of the mass flux for the boundary layer flow. Initial pressure perturbations above the weak interaction solution correspond to compressive downstream disturbances whereas initial pressure perturbations below the weak interaction solution correspond to a downstream expansion such as would occur at the base of an object. The expansive disturbances generate favorable pressure gradients which accelerate the boundary layer without bound until overflow is reached on the computer. For the compressive disturbances, the perturbations lead to adverse pressure gradients in the boundary layer which retard the flow and bring about separation at the point where the curves in figure 3 terminate. These results clearly demonstrate that the onset of separation is an inherent result of a self-sustaining viscid-inviscid interaction. In a complete interaction, see section 3-3, separation will automatically occur provided the final pressure downstream of the compressive disturbance is sufficiently high. The fact that the pressure distribution curve is concave upwards throughout most of the interaction up to separation indicates that the adverse pressure gradient and the increase in displacement thickness are mutually reinforcing.

3-2 Supercritical and subcritical behavior

The concept of supercritical and subcritical flows was first introduced by Crocco (1955). A supercritical flow is stable in nature and can not respond to downstream disturbances. The inviscid pressure area relation for the displacement interaction is one in which thickening of the inviscid region of the boundary layer is associated with a favorable pressure gradient, as in supersonic nozzle flow, with the result that the external flow is deflected towards the wall more than balancing the continued growth of the viscous layer. On the other hand, for subcritical flow the thickening of the total boundary layer is associated with a negative pressure gradient. The external flow is therefore deflected away from the wall producing a rise in pressure which in turn causes a still greater thickening of the boundary layer.

It is evident from these remarks that a supersonic boundary layer is subcritical or supercritical depending on whether or not the viscous growth of the sublayer dominates the streamtube contraction of the supersonic inviscid interaction layer in the presence of a compressive downstream disturbance. Single layer theories provide little insight into the details of this delicate balance since one can not examine the magnitude of the competing mechanisms in each layer. Furthermore, since the interaction problem is highly non-linear it does not follow that an integral average behavior for both layers when lumped together will be nearly the same as if they are treated individually, especially if velocity moments are taken in which the high speed regions are weighted more heavily. The present results show that the difference in behavior is significant and that the supercritical behavior predicated by the single layer

integral theory of Klineberg and Lees (1969) for highly cooled supersonic boundary layers is in fact spurious,

Figures 7a and 7b show graphically the streamtube divergence or convergence between the inner and outer streamlines of the free interaction layer for both adiabatic and highly cooled layers. The three sets of curves given in figure 7a show how the streamline inclination at the edge of the sublayer and the edge of the boundary layer change as the interaction proceeds toward separation for an adiabatic boundary layer at several different Mach numbers. In all three cases one observes that the viscous thickening of the sublayer more than compensates for the adiabatic contraction of the streamtube area that occurs in the inviscid interaction layer. Although the sublayer edge moves outward as the Mach number increases see figures 4, 5 and 6, the streamtube contraction in the inviscid interaction layer (the difference between θ_ϵ and θ_e) grows in importance as the Mach number increases, as shown in curves 3 in figure 7a.

Equivalent results for highly cooled non-adiabatic boundary layer flows are shown in figure 7b. These results show that the difference between θ_ϵ and θ_e is larger for a highly cooled laminar boundary layer than for an adiabatic one at the same Mach number.

The distinction between subcritical and supercritical behavior depends in a large measure on the location of the effective edge of the sublayer. The criterion for choosing the effective sublayer edge has already been discussed at length in section 2-5 where it was shown that good agreement with experiment could be obtained by choosing $\frac{\epsilon_1}{\delta_1}$ to correspond to the maximum in the separation pressure curves shown in figures 4, 5 and 6. Here we are interested in examining how the location of the sublayer edge changes as a function of Mach number for both adiabatic and highly

cooled walls and seeing how this change is reflected in the displacement growth of the sublayer and inviscid interaction layer. The following conclusions can be drawn from these figures:

1. The present numerical experiments show that for both adiabatic and highly cooled wall flows, all solutions are self sustaining and eventually lead to separation if the downstream pressure rise is large enough. Thus, interacting laminar boundary layer flows are apparently always subcritical in nature as is consistent with previous experimental investigations. No supercritical or stable solution has appeared in the present study.

2. For both adiabatic and highly cooled wall flows, the dimensionless sublayer thickness $\frac{\epsilon_1}{\delta_1}$ and separation pressure $\frac{p_s}{p_\infty}$ increase with increasing Mach number. In addition, the separation pressure is a more sensitive function of $\frac{\epsilon_1}{\delta_1}$ as M_∞ increases.

3. For the same M_∞, the dimensionless sublayer thickness $\frac{\epsilon_1}{\delta_1}$ for a highly cooled wall flow is always less than the corresponding adiabatic flow case. On the other hand, the value of the separation pressure for a highly cooled wall flow is higher than the corresponding adiabatic flow at the same Mach number. This is consistent with the experimental observation that a highly cooled wall boundary layer can undergo a higher pressure rise before separating than an adiabatic boundary layer.

In conclusion, the inviscid interaction layer is supercritical for $M_\infty >$ roughly 1.5 whereas the sublayer is always subcritical. The behavior of the total boundary layer depends on whether or not the growth of the sublayer dominates the contraction of the inviscid interaction layer in a compressive disturbance. The results of figure 4 through 7 indicates that all laminar boundary layers, even those with highly cooled walls, are always subcritical since sublayer behavior dominates.

3-3 Complete Interactions

3-3-1 Shock wave induced interaction for adiabatic laminar flow

A comparison of the present numerical solutions with the experimental measurements of Hakkinen et al. (1959) for boundary layer flow in a shock induced interaction at $M_\infty = 2$ and $R_{e\infty} = 1.85 \times 10^5$ is shown in figure 8. Pressure and wall skin friction distributions obtained are in excellent agreement for the interaction region upstream of shock impingement. At the shock impingement point, the velocity profile, enthalpy profile, Mach number profile and the static pressure ratio are taken to be continuous. The streamline angles θ_ϵ and θ_e, however, are discontinuous because the flow streamlines at the boundary layer and sublayer edge are turned by both the incident oblique shock and the reflected expansion fan. For a given shock strength, $\Delta\theta_\epsilon$ and $\Delta\theta_e$ are readily determined using the oblique shock and Prandtl-Meyer wave relations. Thus, all conditions immediately downstream of the point of shock impingement are uniquely determined and the numerical calculations can proceed downstream without further difficulty. The remaining portion of the interaction solution is also in good agreement with the experimental data.

Figure 9 shows the sublayer velocity profiles at various positions for the $M_\infty = 2$ pressure interaction shown in figure 8. These profiles with sublayer edge indicated are plotted for the entire interaction through separation and reattachment. It is obvious that the sublayer velocity profiles are significantly deformed by the viscous effects.

Figure 10 shows the theoretically predicted pressure distribution for a representative adiabatic high Mach number flow at $M_\infty = 10$ and $R_{e\infty} = 7.3 \times 10^5$. The incident oblique shock wave has an inclination angle of 2 degrees. At the shock impingement point, we have assumed again that the streamlines at the boundary layer and sublayer edge are turned through the same angle. The numerical results downstream of shock impingement are very sensitive to the shock turning angle. Two types of downstream behavior are observed in figure 10, one characteristic of a second compressive disturbance further downstream and the second characteristic of a downstream expansion such as would occur at the base of the body. This behavior, of course, parallels the initial value behavior discussed in connection with figure 3. Thus, having selected the point of shock impingement the strength of the shock which allows the solution to proceed smoothly through reattachment is confined to a very narrow band of less than a tenth of a degree. Larger increases in shock strength cause the shock impingement and reattachment points to move further downstream and the length of the separation bubble to increase. Similar results have been obtained by previous investigators, see for example Klineberg and Lees (1969). The plot of the wall shear $\frac{\tau_w}{\frac{1}{2}\rho_\infty u_\infty^2}$ versus distance is also presented in figure 10.

3-3-2 Wedge induced interaction for adiabatic laminar flow

Figure 11 shows the comparison of the present theory with the experimental data obtained by Lewis (1969) for a wedge induced adiabatic laminar boundary layer interaction. The free stream Mach number is $M_\infty = 6.06$ and the free stream Reynolds number $R_{e\infty} = 0.084 \times 10^6$. The wedge angle at the turning corner is 10.25 degrees.

The numerical solutions have been performed (1) with identical flow conditions ($\theta_\infty = 0^\circ$) and (2) with the assumption that the leading edge is at an angle of attack of -0.34 degrees ($\theta_\infty = -0.34^\circ$) or -0.35 degrees ($\theta_\infty = -0.35^\circ$). In figure 11, the small difference in the numerical solutions is not physically important, this difference arises because all solutions are triggered at the same initial starting point but with slightly different initial flow profiles (or equivalently with slightly different initial perturbation pressure gradient). The theoretical pressure distribution curve is in best agreement with the experimental measurements for the case that the leading edge is at an angle of attack of -0.35 degrees. The skin friction predicted by the theory is shown in the same figure. The general agreement shown between theory and experiment is extremely good although the theoretically predicted separated flow region is somewhat shorter than the experimentally observed one.

According to Ko and Kubota (1969) the effect of the angle of attack is to change the static pressure measurements by a constant factor over the whole interaction zone, at least for the small angle range they investigated.

However, the present study shows that the numerical results far downstream of shock impingement point are very sensitive to the initial free stream flow direction at the starting point of interaction. Two types of downstream behavior are observed in figure 11, one characteristic of a second compressive disturbance further downstream and the second characteristic of a downstream expansion disturbance. This phenomenon parallels the initial value behavior mentioned in section 3-3-1 in connection with figure 3.

A comparison with the asymptotic analysis by Stewartson and Williams (1969) is also shown in figure 11. It is evident, that the present theory provides numerical results which are far superior to the lowest order asymptotic analysis.

4 Conclusions

An approximate non-asymptotic analysis has been formulated based on the three layer conceptual model of Lighthill and Stewartson to describe the viscid-inviscid interaction in a laminar boundary layer at finite $R_{e\infty}$. The cornerstone of the analysis is a new interaction equation relating the flow at the outer edge of the sublayer and the flow turning angle in the outer inviscid stream. With appropriate initial profiles specified and novel sublayer outer edge matching conditions satisfied, a continuous solution over the entire interaction field can be obtained by numerically integrating this interaction equation. Numerical results have been obtained and compared with available experimental measurements for both shock induced and wedge induced viscid-inviscid interactions in high speed flights over adiabatic walls. These numerical solutions which are shown in figure 8 and 11 are in very good agreement with the experimental data. Numerical calculations performed at Mach numbers of 2, 4.019 and 10 for both adiabatic and non-adiabatic flows all indicate that viscid-inviscid laminar boundary layer interactions are subcritical in nature.

The results presented in this study have been limited to displacement interactions involving relatively small separated flow regions whose dimensions are roughly of the same order as the interaction distance to separation. For stronger compressive disturbances, the present theoretical model of the sublayer must be modified if one is to obtain a pressure plateau characteristic of extended separated flow regions. The basic difficulty can be surmised from

figure 12 taken from Stewartson and Williams (1973). This figure shows that the quartic velocity profile description for the inner viscous sublayer breaks down in an extended separated flow region. In this figure $x = 0$ is the separation point and $x = -12$ is the start of interaction. Near separation or small x the vorticity profiles are smoothly behaved and the quartic velocity profiles are satisfactory. For large x such as $x = 20.7$ one needs a two region approximation for the u profiles in the sublayer; for example, a quadratic approximation for u near the wall where the shear is linear and a cubic approximation starting at the point where $u = 0$. Such a two region approximation should provide a more realistic profile description of the separated flow in the sublayer and thus enable one to obtain the pressure plateau characteristic of large separated flow regions.

The basic non-linear mathematical model described herein is also applicable to turbulent shock wave boundary layer interactions. The critical new knowledge required for treating turbulent boundary layer interaction problems would appear to be the judicious selection of the velocity and stagnation enthalpy profiles themselves. The same pressure criterion discussed in section 2-8 can be used to determine the edge of the sublayer. One would anticipate from the general characteristics of the turbulent boundary layer velocity profile that the sublayer edge lies somewhere in the buffer zone outside the laminar sublayer and that the inviscid free interaction layer comprises a much larger portion of the total boundary layer thickness than for a laminar boundary layer.

Appendix A

Symbols

a	sonic velocity
h	enthalpy
H	stagnation enthalpy
L	distance from the leading edge of the plate
M	Mach number
P_r	Prandtl number
P	static pressure
R_e	Reynolds number
S	enthalpy function
T	static temperature
u	longitudinal velocity component
U	transformed longitudinal velocity component
v	normal velocity component
V	transformed normal velocity component
x	longitudinal coordinate
X	transformed longitudinal coordinate
y	normal coordinate
Y	transformed normal coordinate
r	ratio of specific heat
η	similarity variable $\eta = \frac{Y}{X}\left(\frac{m+1}{2}\frac{U_e X}{\nu}\right)^{\frac{1}{2}}$
K_{su}	Sutherland's constant
μ	dynamic viscosity
ν	kinematic viscosity $\nu = \frac{\mu}{\rho}$
ρ	mass density
τ	shear stress
ψ	stream function

$$d_{orig} = (1.0 + \frac{r - 1}{2} M_\infty^2)(1.0 + S_w)\frac{0.865}{M_\infty^2} + 0.166\ (r - 1)$$

Subscript

e	local flow outside the boundary layer
w	wall value
$o\infty$	free stream stagnation value

Appendix B

The characteristic x coordinate

The derivation of equation (12) is given below. The characteristic x coordinate depends on the inverse logarithmic decrement of upstream influence Lighthill (1953)

$$\frac{M_e^2}{\sqrt{M_e^2-1}} \int_{\epsilon}^{\delta} \frac{1-M^2}{M^2}\, dy \qquad \text{(B-1)}$$

where the integral is performed across the inviscidly behaving portion of the boundary layer. To determine for compressible flow we introduce the modified Stewartson's transformation employed by Cohen and Reshotko (1959)

$$y = \frac{\rho_\infty}{\rho_e}\frac{a_\infty}{a_e}\sqrt{\frac{2}{m+1}\frac{\nu_\infty x}{u_e}}\int_0^{\eta}\frac{T}{T_\infty}\,d\eta \qquad \text{(B-2)}$$

If one assumes that $\frac{dp}{dx} = 0$ from the leading edge to the beginning of the interaction, then equation (B-2) can be simplified to

$$y = \sqrt{2}\,\frac{x}{\sqrt{R_e}}\int_0^{\eta}\frac{T}{T_e}\,d\eta \qquad \text{(B-3)}$$

where

$$R_e = \frac{\rho_\infty u_\infty x}{\mu_\infty}$$

Thus the boundary layer thickness δ at the beginning of the interaction $x = L$ can be written as

$$\delta = E\,\frac{L}{\sqrt{R_e}} \qquad \text{(B-4)}$$

where

$$E = \sqrt{2}\int_0^{\eta_\delta}\frac{T}{T_e}\,d\eta \qquad \text{(B-5)}$$

We assume the sublayer thickness ϵ can be written in the form

$$\epsilon = I\, L\, R_e^{-K} \tag{B-6}$$

where both I and K have to be determined.

A rough estimate of the integral in (B-1) can be obtained by assuming a linear Mach number profile across the boundary layer, i.e.

$$M(y) = M_e \left(\frac{y}{\delta}\right) \tag{B-7}$$

At $y = \epsilon$ (B-7) reduces to

$$\frac{M_\epsilon}{M_e} = \frac{\epsilon}{\delta} = \frac{I}{E} R_e^{-K+\frac{1}{2}} \tag{B-8}$$

Inserting (B-7) in equation (B-1), performing the integration and using (B-8) one obtains

$$\frac{M_e^2}{\sqrt{M_e^2-1}} \int_\epsilon^\delta \frac{1-M^2}{M^2}\, dy \tag{B-9}$$

$$= \frac{M_e^2}{\sqrt{M_e^2-1}} \left(\frac{1}{M_e^2 \frac{I}{E} R_e^{-K+\frac{1}{2}}} - 1 \right) (\delta - \epsilon)$$

For $\delta >> \epsilon$ and $M_\epsilon M_e << 1$ equation (B-9) simplifies to

$$\frac{M_e^2}{\sqrt{M_e^2-1}} \int_\epsilon^\delta \frac{1-M^2}{M^2}\, dy = \frac{L R_e^{K-1}}{\sqrt{M_e^2-1}} \frac{E^2}{I} \tag{B-10}$$

Equation (B-10) is the desired result given in equation (12).

Appendix C

Interaction equation in terms of Von Mises coordinates

The derivation of equation (52) is given below
The pressure area relation equation (49) for the free interaction layer is given in x , y , coordinates by

$$\tan\theta_e - \tan\theta_\epsilon = -\frac{1}{\rho p}\frac{dp}{dx}\int_\epsilon^\delta \frac{1-M^2}{M^2}\,dy \qquad \text{(C-1)}$$

For the reasons discussed in section 2-4 it is convenient to write (C-1) in terms of Von Mises stream function coordinates (x, ψ). The mass flux per unit area in this region can be expressed as

$$\rho u = \frac{p}{\rho T}u \qquad \text{(C-2)}$$
$$= \left(\frac{\gamma}{R}\right)^{\frac{1}{2}}\frac{P_o}{T_o^{\frac{1}{2}}}\frac{M}{\left(1+\frac{\gamma-1}{2}M^2\right)^{\frac{\gamma+1}{2(\gamma-1)}}}$$

where P_o and T_o are local stagnation conditions.
using the modified Stewartson's transformation equation (57) and equation (C-2) above, we have

$$\frac{\partial\psi}{\partial y} = \frac{\rho u}{\rho_\infty} \qquad \text{(C-3)}$$
$$= (\gamma R T_o)^{\frac{1}{2}}\frac{\rho_o}{\rho_\infty}\frac{M}{\left(1+\frac{\gamma-1}{2}M^2\right)^{\frac{\gamma+1}{2(\gamma-1)}}}$$

Substituting equation (C-3) into (C-1) we get

$$\tan\theta_e - \tan\theta_\epsilon = -\frac{1}{\gamma p^2}\frac{dp}{dx}\frac{p_\infty}{T_\infty}\frac{1}{(\gamma R)^{\frac{1}{2}}}\int_{\psi_\epsilon}^{\psi_\delta}\frac{T^{\frac{1}{2}}(\psi)}{M^3(\psi)}\left(M^2-1\right)d\psi \qquad \text{(C-4)}$$

Equation (C-4) is the interaction equation (52) for the free interaction layer expressed in Von Mises coordinates.

Appendix D

The momentum integral equation for the inner viscous sublayer

The derivation of equation (62) and the transformed boundary conditions (63) in section 2-5 is given below. The equations of motion for a steady two dimensional compressible laminar boundary layer for a perfect gas are:

Continuity equation

$$\frac{\partial(\rho u)}{\partial x} + \frac{\partial(\rho v)}{\partial y} = 0 \tag{D-1}$$

Momentum equations

$$\rho u \frac{\partial u}{\partial x} + \rho v \frac{\partial u}{\partial y} = -\frac{\partial p}{\partial x} + \frac{\partial}{\partial y}\left(\mu \frac{\partial u}{\partial y}\right) \tag{D-2}$$

$$\frac{\partial p}{\partial x} = 0$$

Energy equation

$$\rho u \frac{\partial h}{\partial x} + \rho v \frac{\partial h}{\partial y} = u \frac{\partial p}{\partial x} + \frac{\partial}{\partial y}\left(\frac{\mu}{P_r}\frac{\partial h}{\partial y}\right) + \mu\left(\frac{\partial u}{\partial y}\right)^2 \tag{D-3}$$

Applying the modified Stewartson's transformation equation (57) to the boundary layer equations (D-1), (D-2) and (D-3) and assuming that P_r and C_p are constant, one obtains the following equations

$$\frac{\partial U}{\partial X} + \frac{\partial V}{\partial Y} = 0 \tag{D-4}$$

$$U \frac{\partial U}{\partial X} + V \frac{\partial U}{\partial Y} = U_e \frac{dU_e}{dX}(1+\Lambda) + \nu_\infty \frac{\partial^2 U}{\partial Y^2} \tag{D-5}$$

The transformed normal velocity component v, can be replaced by

$$V = -\int_0^Y \frac{\partial U}{\partial X}\, dY$$

as seen from the continuity equation. Consequently, we have an alterate form for equation (D-5)

$$U\frac{\partial U}{\partial X} - \frac{\partial U}{\partial Y}\int_0^Y \frac{\partial U}{\partial X}\, dY = U_e \frac{dU_e}{dX}(1+S) + \nu_\infty \frac{\partial^2 U}{\partial Y^2} \qquad \text{(D-6)}$$

Integrating the equation of motion (D-6) with respect to Y from Y = 0 (wall) to Y = E (sublayer edge), we have

$$\int_0^E \left(U\frac{\partial U}{\partial X} - \frac{\partial U}{\partial Y}\int_0^Y \frac{\partial U}{\partial X}\, dY\right) dY = U_e \frac{dU_e}{dX}\int_0^E (1+S)\, dY + \nu_\infty \frac{\partial U}{\partial Y}\Big|_0^E = RHS \qquad \text{(D-7)}$$

Integrating by parts, we have for the second term

$$\int_0^E \frac{\partial U}{\partial Y}\left(\int_0^Y \frac{\partial U}{\partial X}\, dY\right) dY = U_E \int_0^E \frac{\partial U}{\partial X}\, dY - \int_0^E U\frac{\partial U}{\partial X}\, dY \qquad \text{(D-8)}$$

so that

$$\int_0^E \left(U\frac{\partial U}{\partial X} - U_E\frac{\partial U}{\partial X} + U\frac{\partial U}{\partial X}\right) dY = RHS \ (D\text{-}7) \qquad \text{(D-9)}$$

which can be contracted to

$$\int_0^E \frac{\partial}{\partial X}\left(U(U_E - U)\right) dY - \int_0^E U\frac{\partial U_E}{\partial X}\, dY = -RHS \ (D\text{-}7) \qquad \text{(D-10)}$$

Taking the differentiation outside the integral in equation (D-10) we have

$$\frac{\partial}{\partial X}\int_0^E U(U_E - U)\, dY + \frac{dU_E}{dX}\int_0^E (U_E - U)\, dY$$

$$- \frac{dU_E}{dX}\int_0^E U_E\, dY = -RHS \ (D\text{-}7) \qquad \text{(D-11)}$$

We now define the sublayer displacement thickness δ^* and the sublayer momentum thickness θ^* by

$$\theta^* U_E^2 = \int_0^E U(U_E - U)\, dy \tag{D-12}$$

and

$$\delta^* U_E = \int_0^E (U_E - U)\, dy \tag{D-13}$$

Introducing these definitions in equation (D-11) we have

$$\frac{\partial \theta^*}{\partial X} + \frac{\theta^*}{U_E}\frac{dU_E}{dX}\left(2 + \frac{\delta^*}{\theta^*} - \frac{E}{\theta^*} - \frac{U_e}{U_E}\frac{\frac{dU_e}{dX}}{\frac{dU_E}{dX}}\right) \frac{1}{\theta^*}\int_0^E (1+S)\, dy$$

$$- \frac{\nu_\infty}{U_E^2}\frac{\tau_E}{\mu_E} + \frac{\nu_\infty}{U_E^2}\frac{\tau_w}{\mu_w} = 0 \tag{D-14}$$

This is the momentum integral equation for the two dimensional compressible viscous sublayer.

The boundary conditions at $y = 0$ for the sublayer profiles are given by equations (31) and (32).

$$\text{at } y=0; \quad u = 0, \ \frac{\partial}{\partial y}\left(\mu \frac{\partial u}{\partial y}\right) = \frac{dp}{dx}, \ \frac{\partial^2}{\partial y^2}\left(\mu \frac{\partial u}{\partial y}\right) = 0$$

$$H = H_w, \ \frac{\partial}{\partial y}\left(\mu \frac{\partial H}{\partial y}\right) = 0 \tag{D-15}$$

When written in the transformed coordinate Y the boundary conditions on U become

$$\text{at } Y=0; \quad U = 0, \ \frac{\partial^2 U}{\partial Y^2} = \frac{\frac{dp}{dX}}{\mu_\infty \left(\frac{T_e}{T_\infty}\right)^{\frac{3}{2}} \frac{\rho}{\rho_\infty}\frac{f_w}{f_\infty}}$$

$$\frac{\partial^3 U}{\partial Y^3} - \frac{1}{T_w}\frac{\partial T}{\partial Y}\frac{\partial^2 U}{\partial Y^2} = 0 \tag{D-16}$$

While those on H reduce to

$$\text{at } Y = 0 \; ; \quad H = H_w \; , \quad \frac{\partial^2 H}{\partial Y^2} = 0 \tag{D-17}$$

For non-adiabatic flow it is convenient to define a stagnation enthalpy ratio function $S = \frac{H}{H_e} - 1$ instead of the local stagnation enthalpy H , where H_e is the free stream stagnation enthalpy. In terms of S , the corresponding boundary conditions for the enthalpy function are

$$\text{at } Y = 0 \; ; \quad S = S_w \; , \quad \frac{\partial^2 S}{\partial Y^2} = 0 \tag{D-18}$$

Appendix E

The new profiles for the inner viscous sublayer

In this appendix we derive the profile coefficients of equations (69) and (70) in the text. We seek to construct a suitable family of velocity and stagnation enthalpy profiles for the sublayer which satisfy the wall and edge conditions specified by equations (63), (64) and (65). These profiles given by equations (66) - (70) were obtained as follows: For the velocity profile we assume a fourth order polynomial of the form

$$\frac{u}{u_e} = A\xi + B\xi^2 + C\xi^3 + D\xi^4 \qquad \text{(E-1)}$$

Where $\xi = \frac{y}{\epsilon}$ is a scaled normal coordinate which varies between $0 \leq \xi \leq 1$ in the sublayer. Similarly, for the stagnation enthalpy ratio S we assume a third order polynomial of the form

$$S = \bar{A} + \bar{B}\xi + \bar{C}\xi^2 + \bar{D}\xi^3 \qquad \text{(E-2)}$$

The afore mentioned wall compatibility conditions and the matching conditions at the sublayer edge (equation (63) - (65)) are sufficient to determine the coefficient constants A, B, C, D, $\bar{A}$, $\bar{B}$, $\bar{C}$ and $\bar{D}$.
Introducing the dimensionless quantity

$$\Lambda = \frac{\frac{dp}{dx}}{\mu_\infty \frac{u_e}{\epsilon^2}\left(\frac{T_e}{T_\infty}\right)^{\frac{3}{2}} \frac{p}{p_\infty} \frac{f_w}{f_\infty}} \qquad \text{(E-3)}$$

we have the following relations:

$$A + B + C + D = 1$$

$$A + 2B + 3C + 4D = \frac{\partial(\frac{U}{U_e})}{\partial \xi} \text{ at } \xi = 1$$

$$2B = -\Lambda$$

$$6C = \frac{\bar{B}}{1 + S_w} \qquad \text{(E-4)}$$

$$\bar{A} = S_w$$

$$2\bar{C} = 0$$

$$\bar{A} + \bar{B} + \bar{C} + \bar{D} = S \text{ at } \xi = 1$$

$$\bar{B} + 2\bar{C} + 3\bar{D} = \frac{\partial S}{\partial \xi} \text{ at } \xi = 1$$

The simultaneous solutions of the above equations give the following expressions for the coefficients in equations (E-1) and (E-2)

$$A = \frac{4}{3} - \frac{2}{3}B - \frac{1}{3}C - \frac{1}{3}\frac{\partial(\frac{U}{U_e})}{\partial \xi} \text{ at } \xi = 1$$

$$B = -\frac{\Lambda}{2}$$

$$C = -\frac{\Lambda}{6}\frac{\bar{B}}{1+S_w} \qquad \text{(E-5)}$$

$$D = -\frac{1}{3} - \frac{B}{3} - \frac{2}{3}C + \frac{1}{3}\frac{\partial(\frac{U}{U_e})}{\partial \xi} \text{ at } \xi = 1$$

$$\overline{A} = S_w$$

$$\overline{B} = \frac{3}{2} S_{at\,\xi=1} - \frac{3}{2} S_w - \frac{1}{2} \frac{dS}{d\xi} at\ \xi=1 \qquad \text{(E-6)}$$

$$\overline{C} = 0$$

$$\overline{D} = \frac{1}{2} S_w - \frac{1}{2} S_{at\,\xi=1} + \frac{1}{2} \frac{dS}{d\xi} at\ \xi=1$$

These results for the profile coefficients are equations (69) and (70) in the text.

Appendix F

The expression for $\tan \theta_\epsilon$

In this appendix we derive equation (73) in the text. The steady two-dimensional compressible boundary layer continuity equation is

$$\frac{\partial}{\partial x}\rho u + \frac{\partial}{\partial y}\rho v = 0 \tag{F-1}$$

Upon integrating equation (F-1) with respect to y, from $y = 0$ (wall) to y, we obtain

$$\rho v = -\int_0^y \frac{\partial}{\partial x}\rho u \, dy \tag{F-2}$$

The cooresponding value of (F-2) evaluated at the sublayer edge $y = \epsilon$ is

$$\rho_\epsilon v_\epsilon = -\int_0^\epsilon \frac{\partial(\rho u)}{\partial x} dy \tag{F-3}$$

$$\tan\theta_\epsilon = \frac{v_\epsilon}{u_\epsilon} = \frac{\rho_\epsilon v_\epsilon}{\rho_\epsilon u_\epsilon} = \frac{-\int_0^\epsilon \frac{\partial}{\partial x}\rho u \, dy}{\rho_\epsilon u_\epsilon} \tag{F-4}$$

We next introduce the modified Stewartson's transformation

$$dY = \frac{a_e \rho_e}{a_\infty \rho_\infty} dy$$

$$U = \frac{a_\infty}{a_e} u$$

and let $\xi = \frac{Y}{E}$

Equation (F-4) in terms of these transformed variables becomes

$$\tan\theta_\epsilon = \frac{-\int_0^E \frac{d}{dx}\rho u\, dy \;\frac{a_\infty}{a_e}\frac{\rho_\infty}{\rho}}{\rho_\epsilon U_E \;\frac{a_e}{a_\infty}}$$

$$= \frac{-\int_0^{\xi} \frac{d}{dx}\rho u\, d\xi \;\frac{\rho_\infty}{\rho} E}{\rho_\epsilon U_E \left(\frac{a_e}{a_\infty}\right)^2} \qquad \text{(F-5)}$$

Equation (F-5) is result (73) in the text.

Appendix G

The transformed momentum thickness expressed in terms of the sublayer velocity profile

The derivation of equation (93) is given below. As shown in appendix D, the transformed momentum thickness θ^* has the form

$$\theta^* = \int_0^{\varepsilon} \frac{u}{u_e}\left(1-\frac{u}{u_e}\right) dy \qquad \text{(D-12)}$$

or

$$\theta^* = \varepsilon \int_0^1 \frac{u}{u_e}\left(1-\frac{u}{u_e}\right) d\xi \quad , \xi = \frac{y}{\varepsilon} \qquad \text{(G-1)}$$

In the inner viscous sublayer the assumed form for the velocity profile is (see equation (69))

$$\frac{u}{u_e} = A\xi + B\xi^2 + C\xi^3 + D\xi^4 \qquad \text{(E-1)}$$

where

$$\Lambda = \frac{-\frac{d(\frac{p}{p_\infty})}{d(\frac{x}{\delta_1})} Re_\infty \frac{\delta_1}{x_1} \frac{T_w}{T_\infty}\left(1+\frac{\gamma-1}{2}M_\infty^2\right)^{\frac{\gamma+1}{\gamma-1}}}{\gamma \frac{p}{p_\infty}\left(\frac{T_e}{T_\infty}\right)^{\frac{3}{2}} M_e M_\infty} \frac{\left(\frac{\varepsilon}{\delta_1}\right)^2}{\left(\frac{\varepsilon}{u_e}\right)^2}$$

$$A = \frac{1}{3} + \left(\frac{1}{3} + \frac{1}{18}\frac{\bar{B}}{1+s_w}\right)\Lambda - \frac{1}{3}\left.\frac{d(\frac{u}{u_e})}{d\xi}\right|_{at\ \xi=1} = A_1 + A_2\Lambda + A_3$$

$$B = -\frac{1}{2}\Lambda = B_1\Lambda$$

$$C = -\frac{\Lambda}{6}\frac{\bar{B}}{1+s_w} = C_1\Lambda$$

$$D = -\frac{1}{3} + \left(\frac{1}{6} + \frac{1}{9}\frac{\bar{B}}{1+s_w}\right)\Lambda + \frac{1}{3}\left.\frac{d(\frac{u}{u_e})}{d\xi}\right|_{at\ \xi=1} = D_1 + D_2\Lambda + D_3$$

$$\bar{B} = \frac{1}{2}\left(3\int_{\partial\Omega_{\xi=1}} - 3\int_{W} - \frac{d\delta}{d\xi}\,d\Omega_{\xi=1}\right)$$

Inserting equation (E-1) into equation (G-1) we have

$$\theta^* = E(\alpha_1 + \alpha_2\Lambda + \alpha_3)$$

where

$$\alpha_1 = -\frac{A_1}{2} - \frac{A_3}{2} - \frac{D_1}{5} - \frac{D_3}{5} + \frac{A_1^2}{3} + \frac{A_3^2}{3} + \frac{2}{3}A_1A_3 + \frac{D_1^2}{9} + \frac{D_3^2}{9} + \frac{2}{9}D_1D_3 + \frac{2}{6}A_1D_1 + \frac{2}{6}A_1D_3 + \frac{2}{6}A_3D_1 + \frac{2}{6}A_3D_3$$

$$\alpha_2 = -\frac{A_2}{2} - \frac{B_1}{3} - \frac{C_1}{4} - \frac{D_2}{5} + \frac{2}{3}A_1A_2 + \frac{2}{3}A_2A_3 + \frac{2}{9}D_1D_2 + \frac{2}{9}D_2D_3 + \frac{2}{4}A_1B_1 + \frac{2}{4}A_3B_1 + \frac{2}{5}A_1C_1 + \frac{2}{5}A_3C_1 + \frac{2}{6}A_1D_2 + \frac{2}{6}A_2D_1 + \frac{2}{6}A_2D_3 + \frac{2}{6}A_3D_2 + \frac{2}{7}B_1D_1 + \frac{2}{7}B_1D_3 + \frac{2}{8}C_1D_1 + \frac{2}{8}C_1D_3$$

$$\alpha_3 = \frac{A_2^2}{3} + \frac{B_1^2}{5} + \frac{C_1^2}{7} + \frac{D_2^2}{9} + \frac{2}{4}A_2B_1 + \frac{2}{5}A_2C_1 + \frac{2}{6}A_2D_2 + \frac{2}{6}B_1C_1 + \frac{2}{7}B_1D_2 + \frac{2}{8}C_1D_2$$

These results are equation (93) in the text.

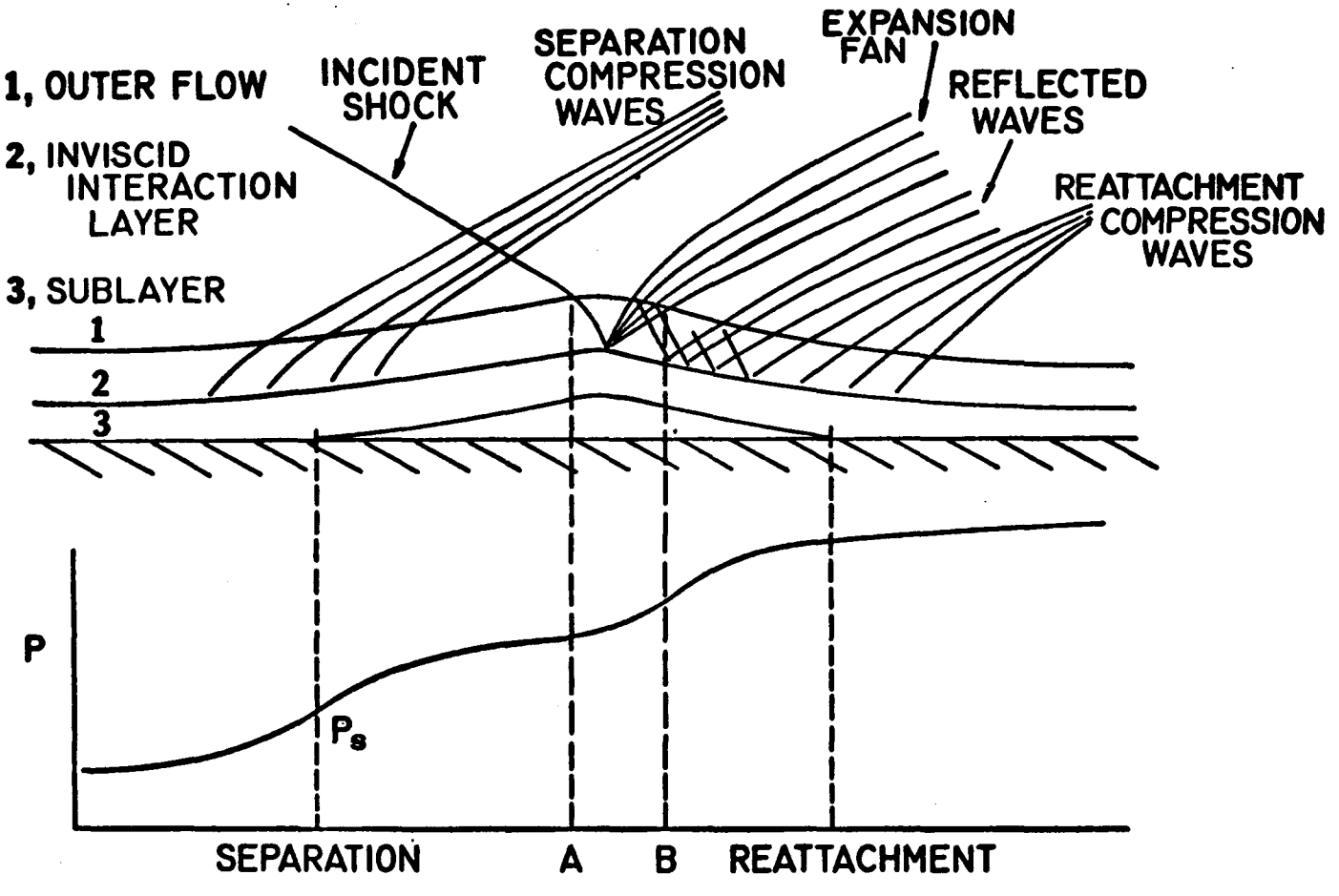

FIG. 1 SCHEMATIC OF FLOW PATTERN

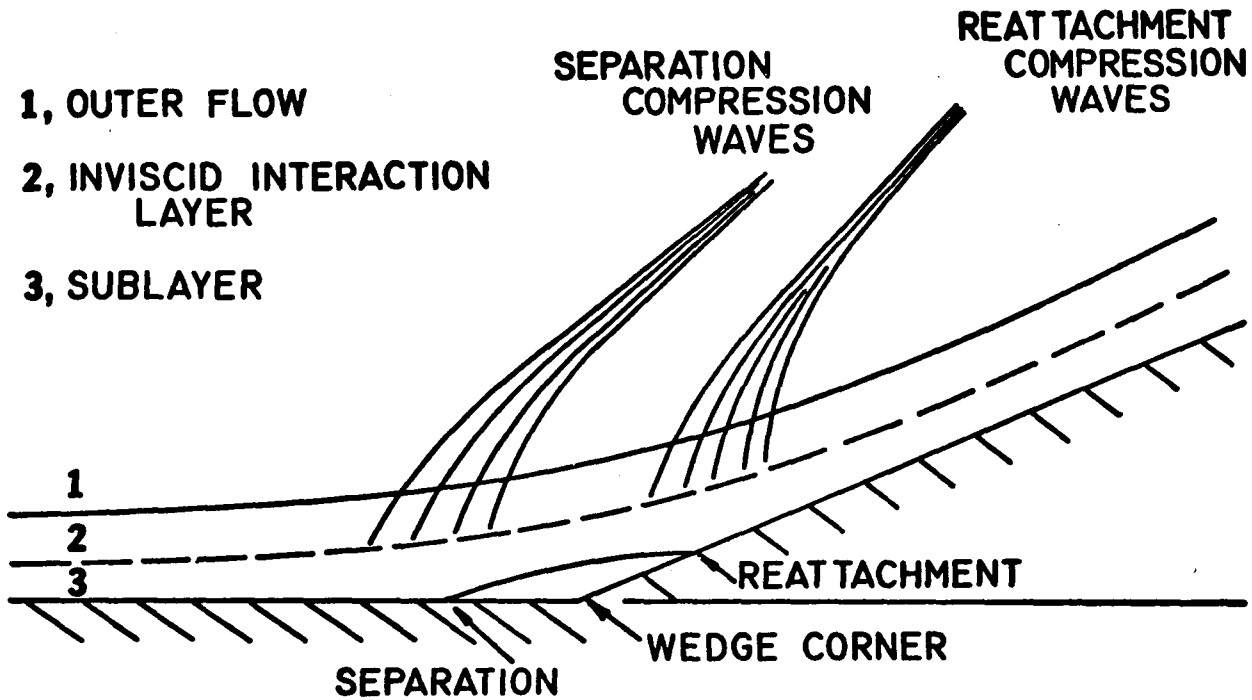

FIG. 2 WEDGE INDUCED VISCID INVISCID FLOW INTERACTION

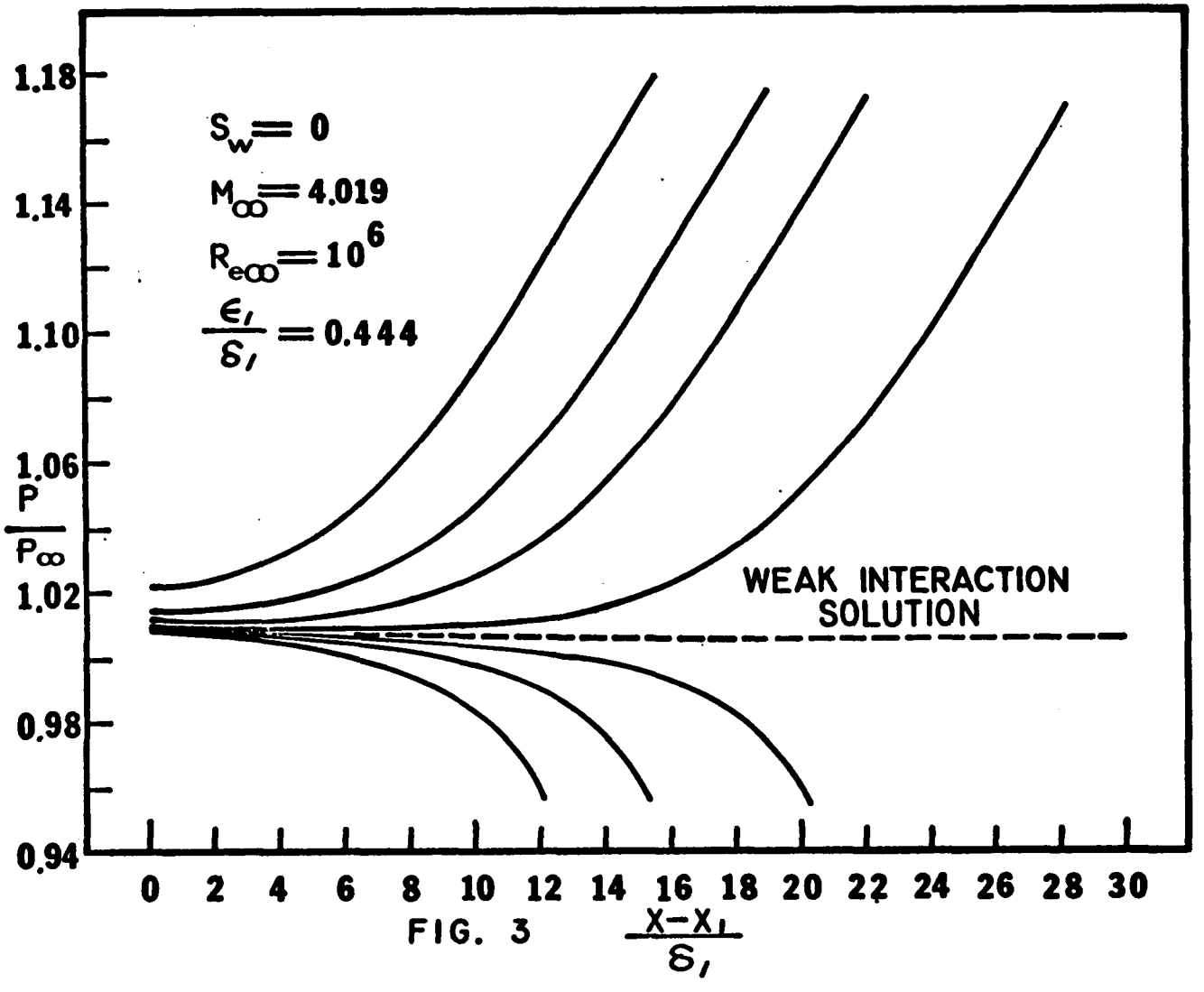
1.18
1.14
1.10
1.06
1.02
0.98
0.94
P/P∞
$S_w = 0$
$M_\infty = 4.019$
$R_{e\infty} = 10^6$
$\epsilon_1/\delta_1 = 0.444$
WEAK INTERACTION SOLUTION
0 2 4 6 8 10 12 14 16 18 20 22 24 26 28 30
$(X-X_L)/\delta_1$

FIG. 3

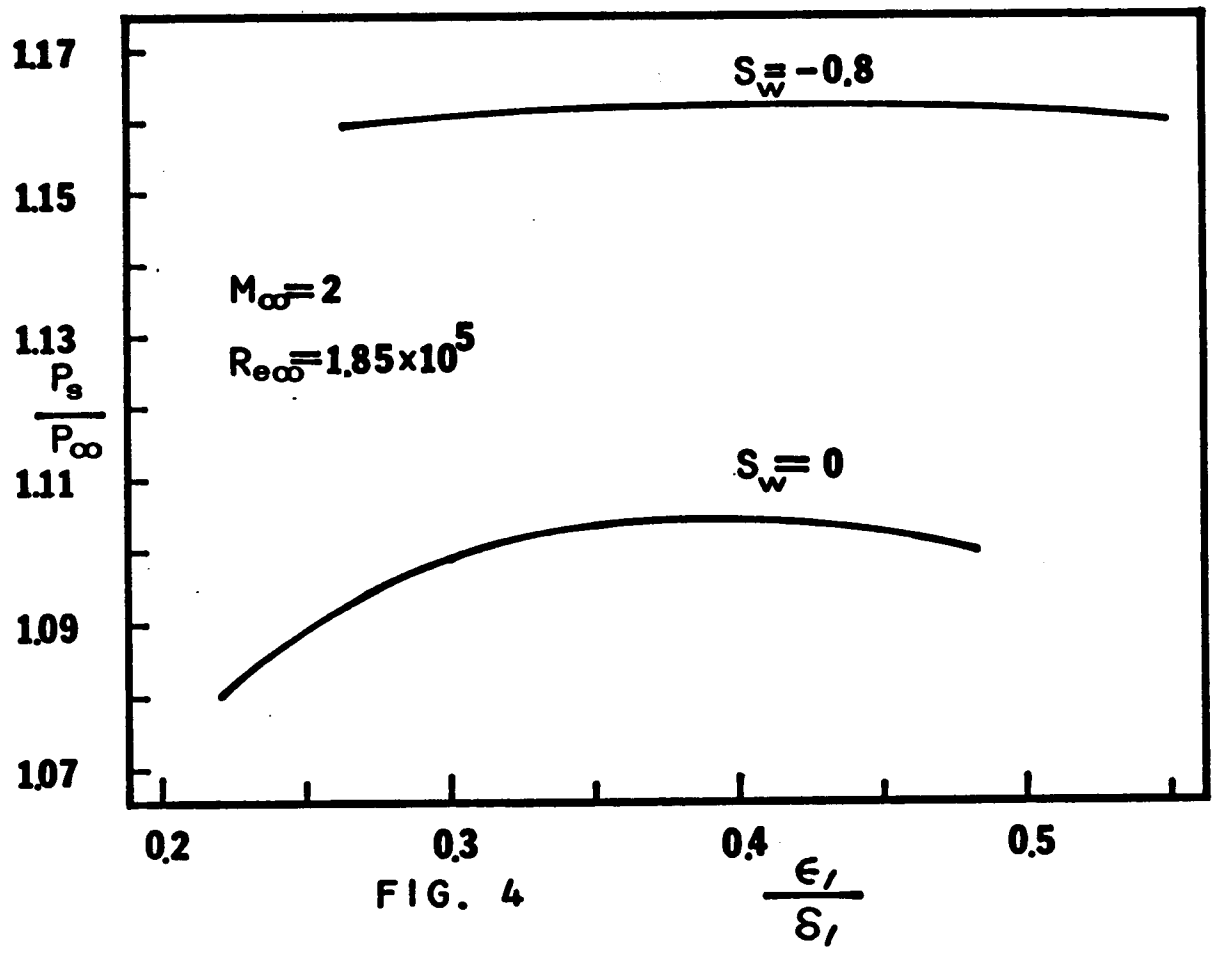
1.17
1.15
1.13
1.11
1.09
1.07
$\frac{P_s}{P_\infty}$
$S_w = -0.8$
$M_\infty = 2$
$R_{e\infty} = 1.85 \times 10^5$
$S_w = 0$
0.2
0.3
0.4
0.5
$\frac{\epsilon_1}{\delta_1}$

FIG. 4

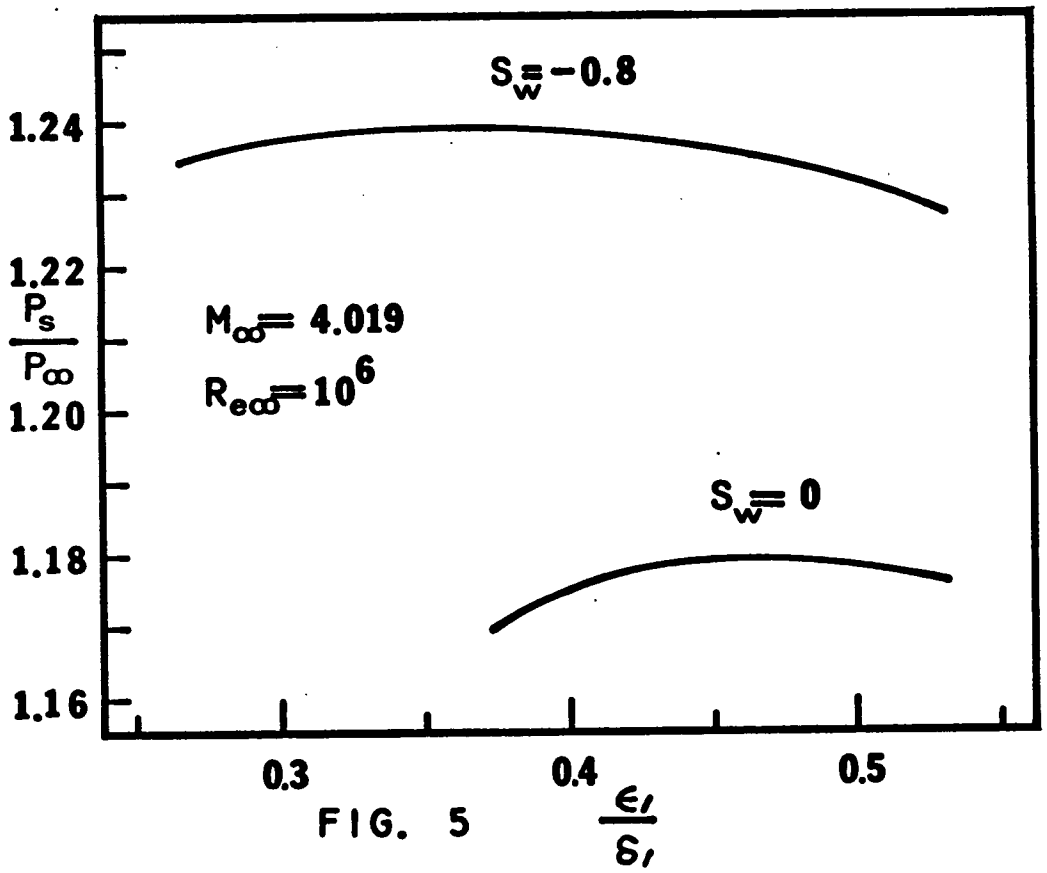
$S_w = -0.8$
1.24
1.22
$\frac{P_s}{P_\infty}$
$M_\infty = 4.019$
$Re_\infty = 10^6$
1.20
$S_w = 0$
1.18
1.16
0.3
0.4
0.5
$\frac{\epsilon_1}{\delta_1}$

FIG. 5

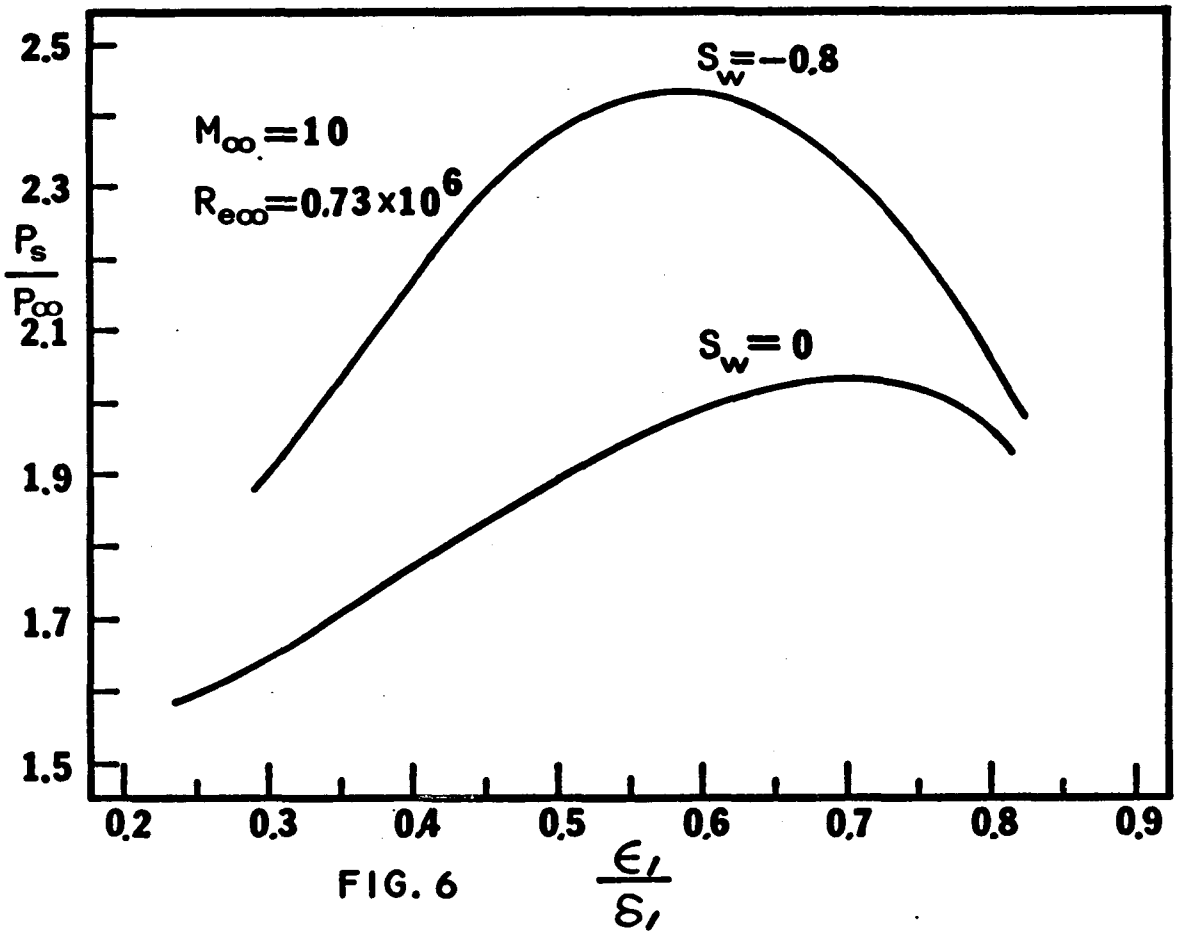
2.5
2.3
2.1
1.9
1.7
1.5
$\frac{P_s}{P_\infty}$
$S_w = -0.8$
$M_\infty = 10$
$R_{e\infty} = 0.73 \times 10^6$
$S_w = 0$
0.2
0.3
0.4
0.5
0.6
0.7
0.8
0.9
$\frac{\epsilon_1}{\delta_1}$

FIG. 6

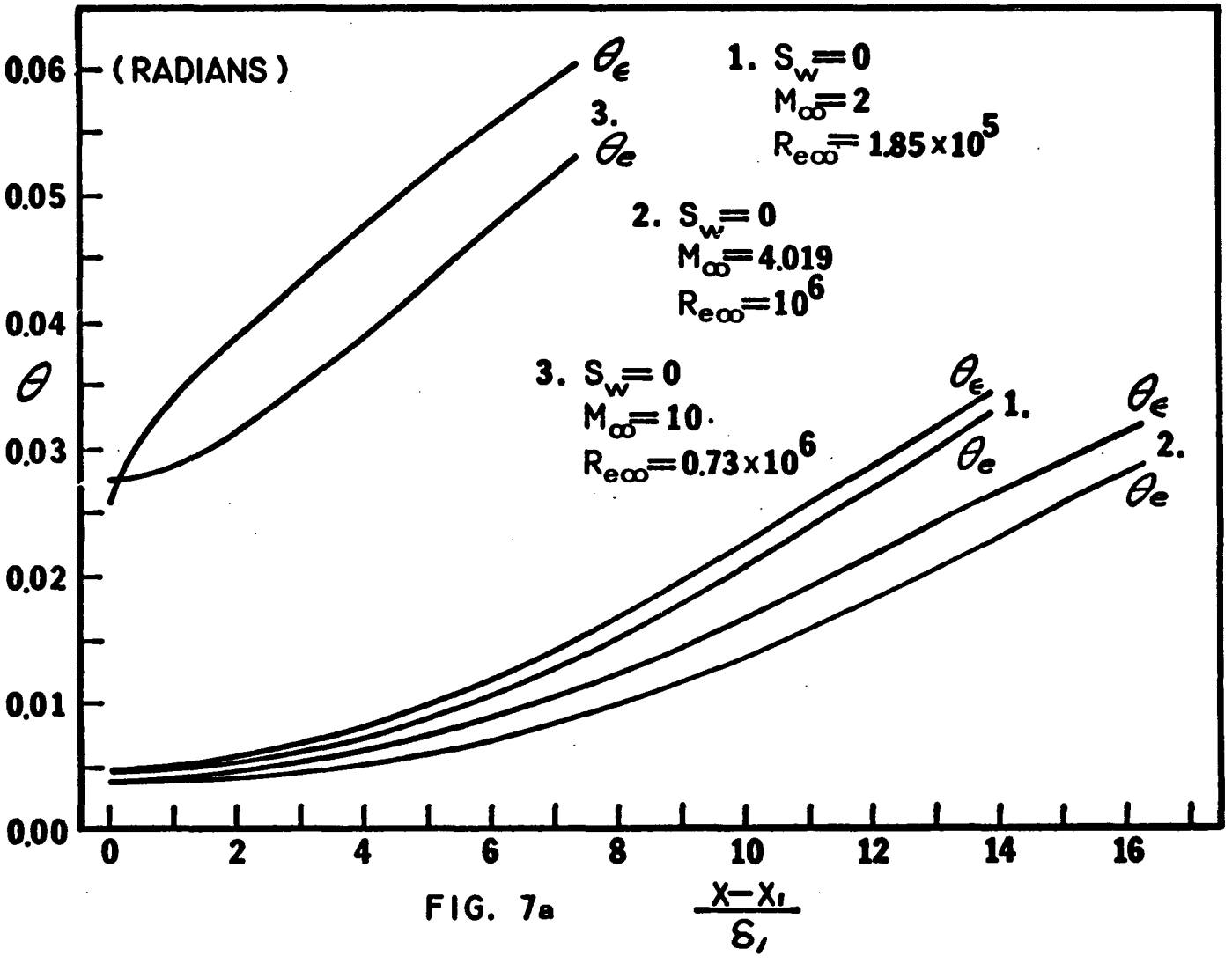
0.06
(RADIANS)
0.05
0.04
θ
0.03
0.02
0.01
0.00
0
2
4
6
8
10
12
14
16
X−X₁ / δ₁
θe
3.
θe
1. S_w = 0
M∞ = 2
R_e∞ = 1.85 x 10^5
2. S_w = 0
M∞ = 4.019
R_e∞ = 10^6
3. S_w = 0
M∞ = 10.
R_e∞ = 0.73 x 10^6
θe
1.
θe
θe
2.
θe

FIG. 7a

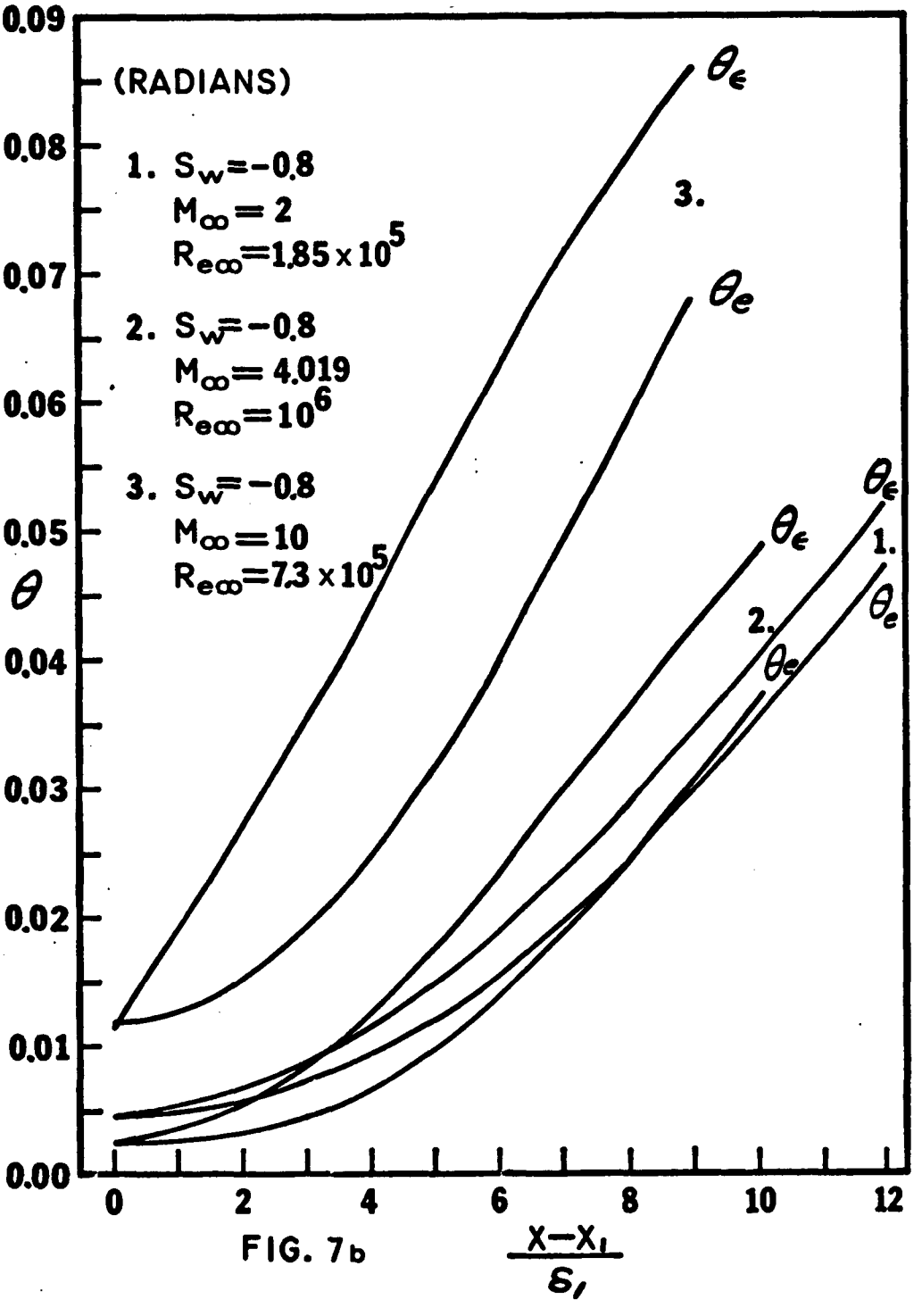
0.09
0.08
0.07
0.06
0.05
0.04
0.03
0.02
0.01
0.00
θ
(RADIANS)
1. S_w=-0.8
M_∞ = 2
$R_{e\infty}$=1.85 x 10^5
2. S_w=-0.8
M_∞ = 4.019
$R_{e\infty}$=10^6
3. S_w=-0.8
M_∞ = 10
$R_{e\infty}$=7.3 x 10^5
θ_ϵ
θ_e
3.
2.
1.
0
2
4
6
8
10
12
$\frac{X-X_1}{\delta_1}$

FIG. 7b

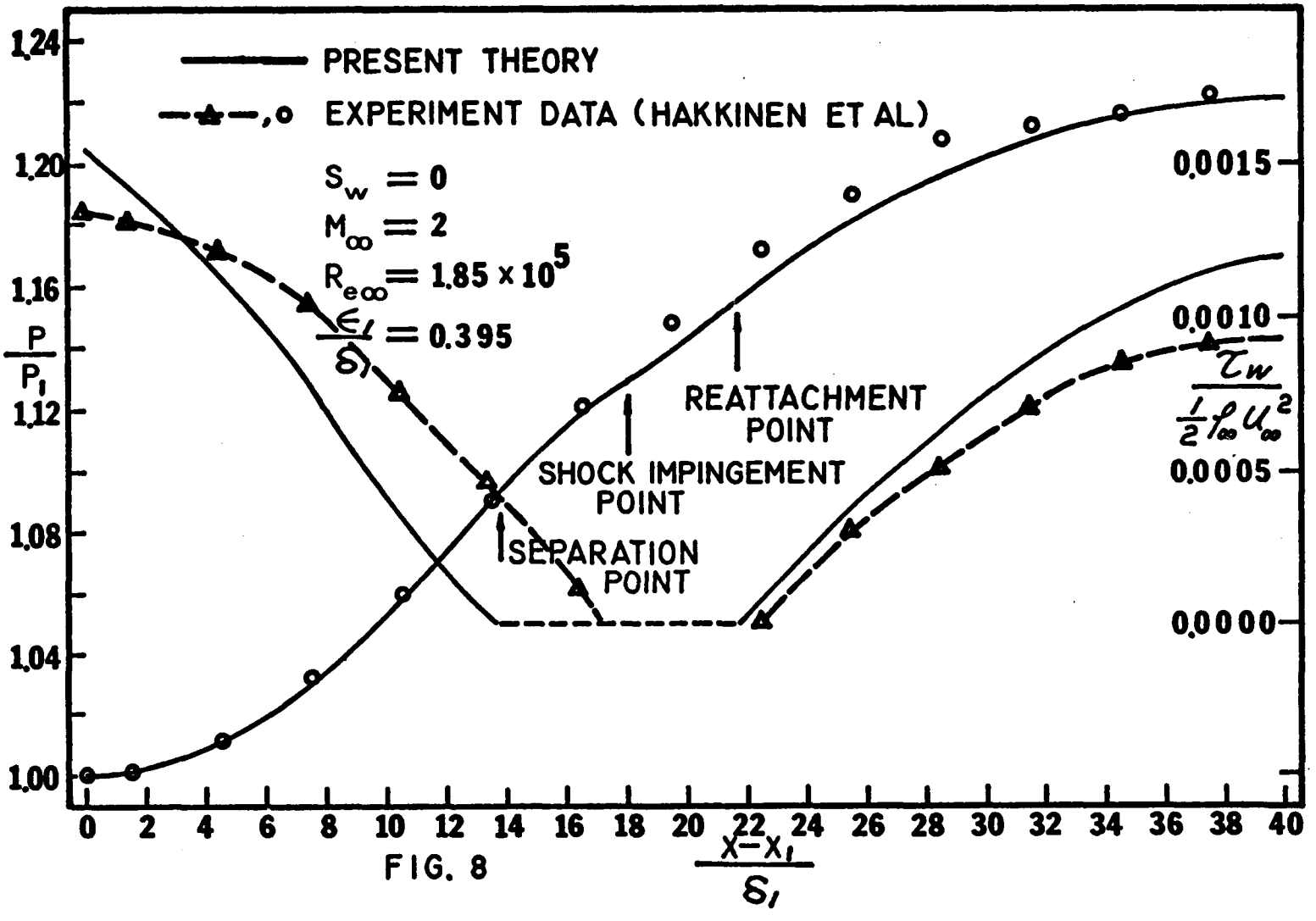
PRESENT THEORY
EXPERIMENT DATA (HAKKINEN ET AL)
$S_w = 0$
$M_\infty = 2$
$R_{e\infty} = 1.85 \times 10^5$
$\frac{\epsilon_1}{\delta_1} = 0.395$
REATTACHMENT POINT
SHOCK IMPINGEMENT POINT
SEPARATION POINT
$\frac{P}{P_1}$
$\frac{\tau_w}{\frac{1}{2}\rho_\infty U_\infty^2}$
$\frac{X-X_1}{\delta_1}$
1.24
1.20
1.16
1.12
1.08
1.04
1.00
0.0015
0.0010
0.0005
0.0000
0 2 4 6 8 10 12 14 16 18 20 22 24 26 28 30 32 34 36 38 40

FIG. 8

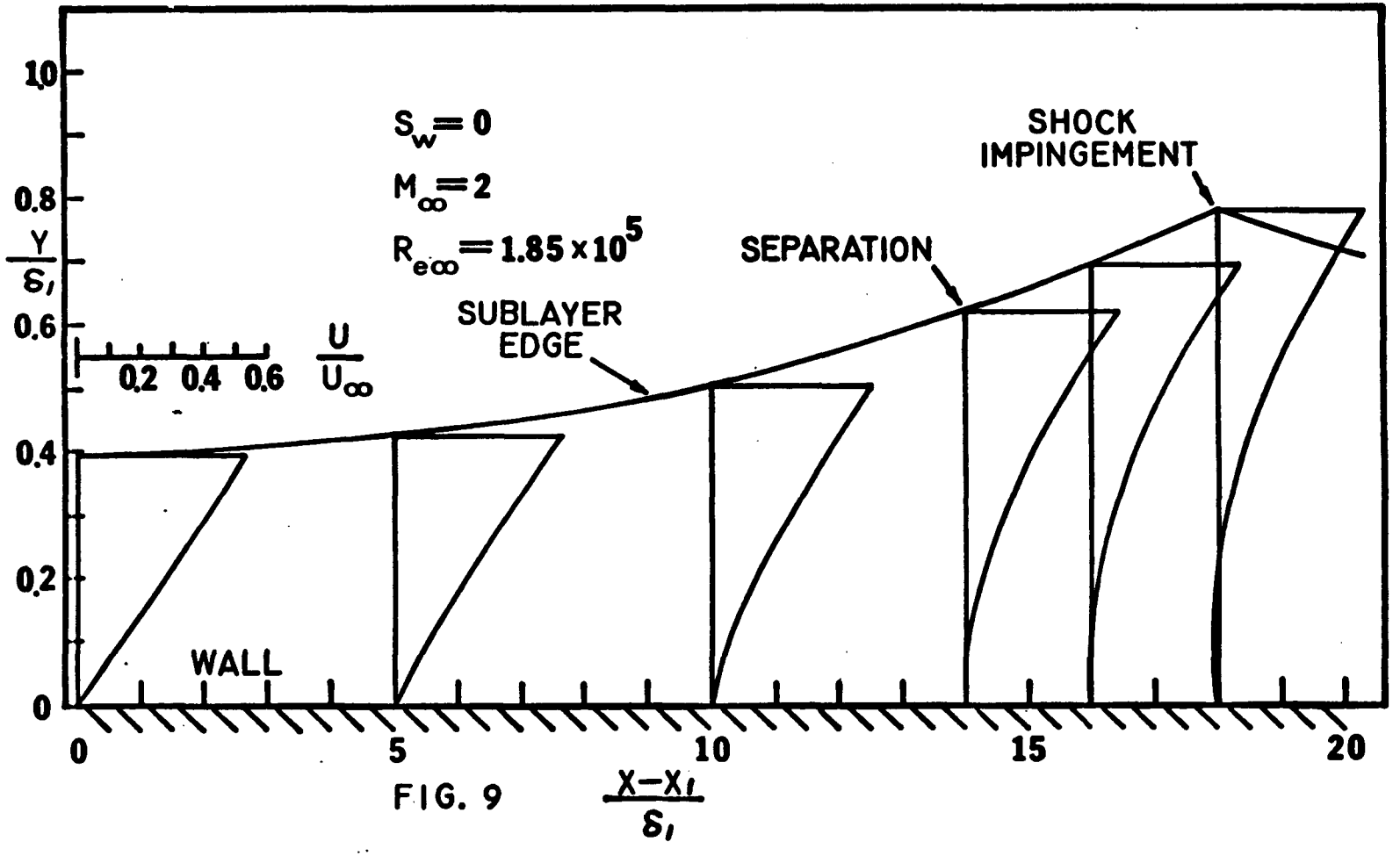
$S_w = 0$
$M_\infty = 2$
$R_{e\infty} = 1.85 \times 10^5$
SHOCK IMPINGEMENT
SEPARATION
SUBLAYER EDGE
WALL
$\frac{U}{U_\infty}$
0.2 0.4 0.6
$\frac{Y}{\delta_1}$
1.0
0.8
0.6
0.4
0.2
0
0
5
10
15
20
$\frac{X-X_1}{\delta_1}$

FIG. 9

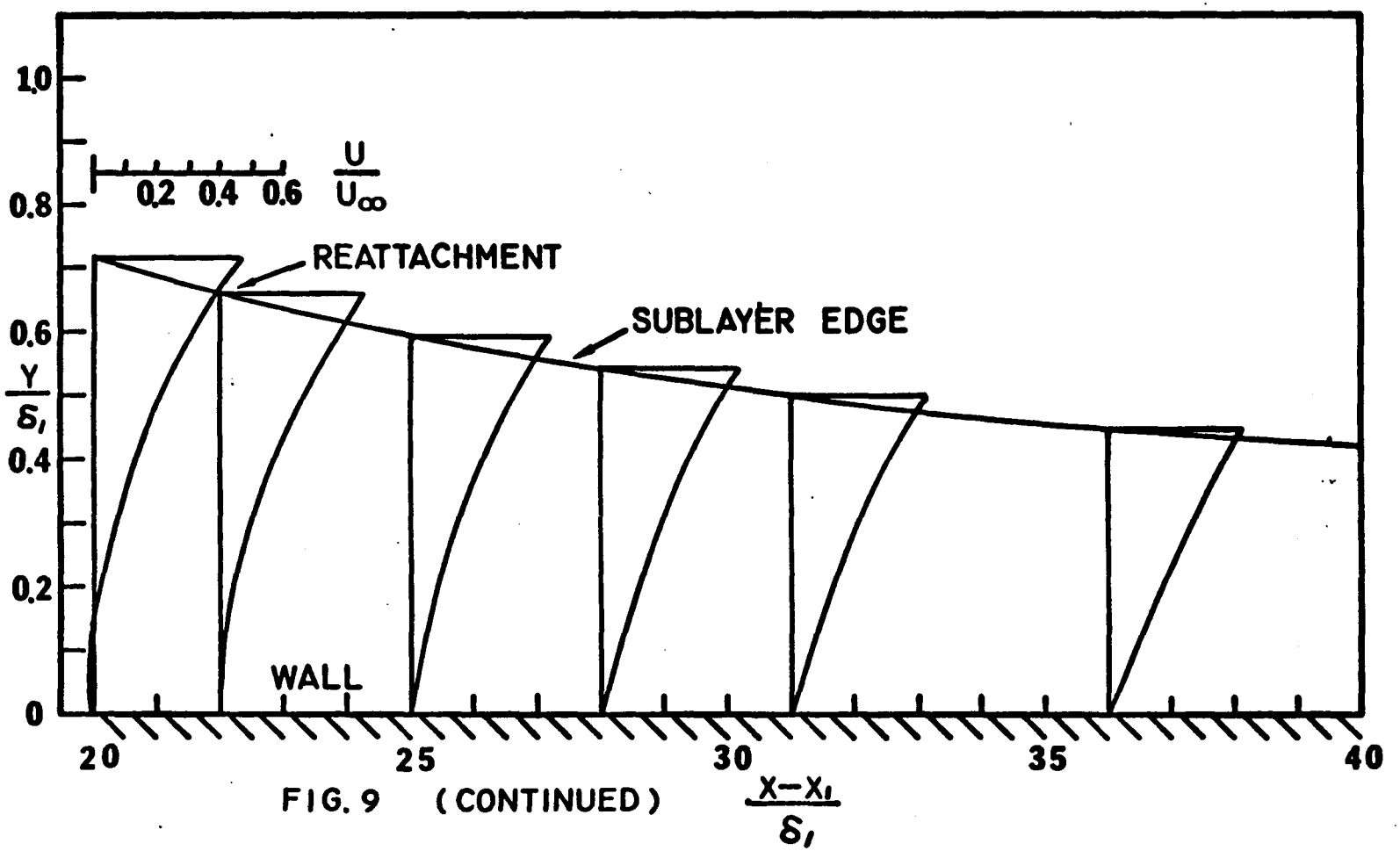

FIG. 9 (CONTINUED)

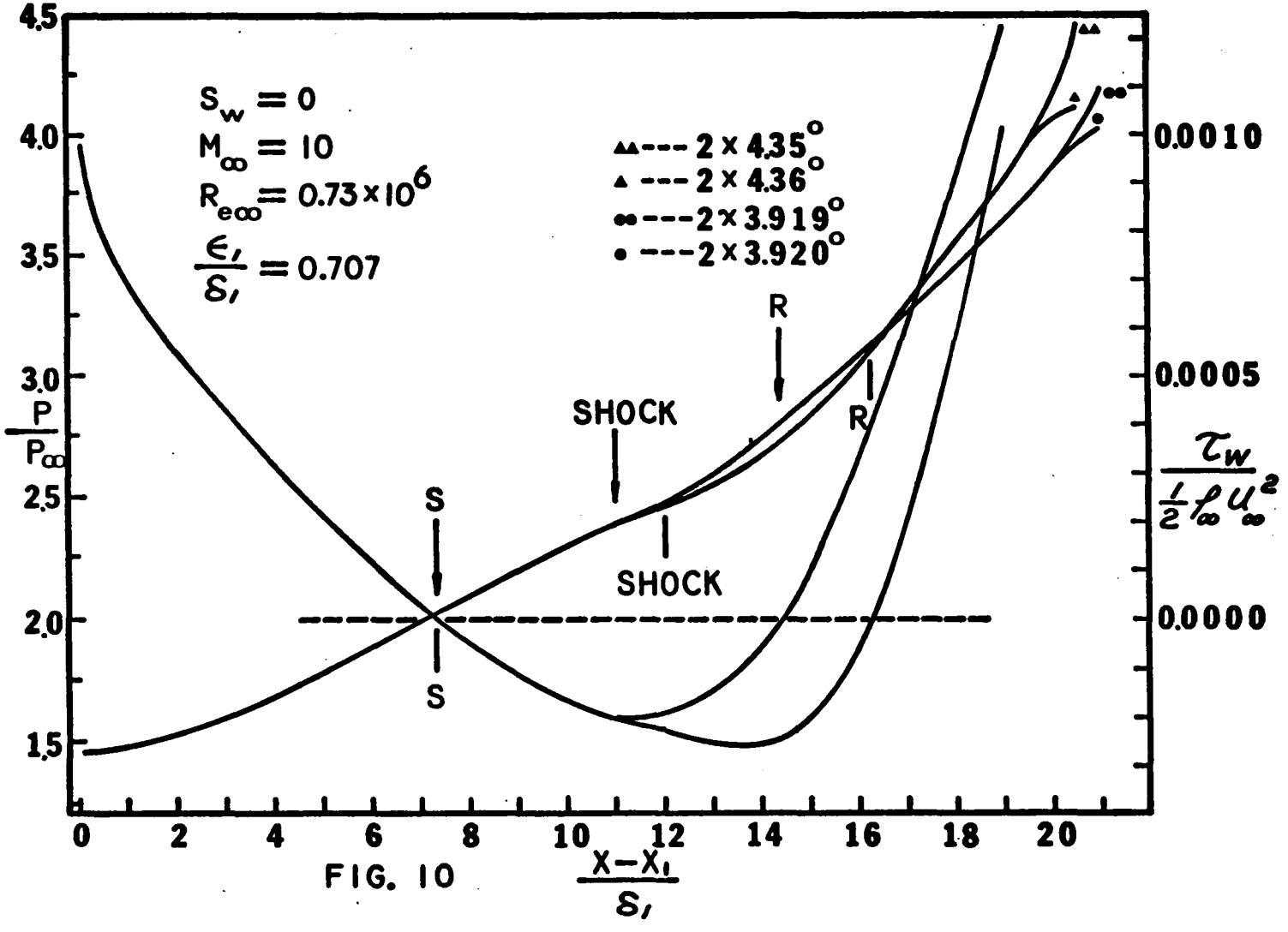
$S_w = 0$
$M_\infty = 10$
$R_{e\infty} = 0.73 \times 10^6$
$\frac{\epsilon_1}{\delta_1} = 0.707$
▲▲--- 2 × 4.35°
▲ --- 2 × 4.36°
●● --- 2 × 3.919°
● --- 2 × 3.920°
R
R
SHOCK
SHOCK
S
S
4.5
4.0
3.5
3.0
2.5
2.0
1.5
$\frac{P}{P_\infty}$
0.0010
0.0005
0.0000
$\frac{\tau_w}{\frac{1}{2}\rho_\infty U_\infty^2}$
0
2
4
6
8
10
12
14
16
18
20
$\frac{X - X_1}{\delta_1}$

FIG. 10

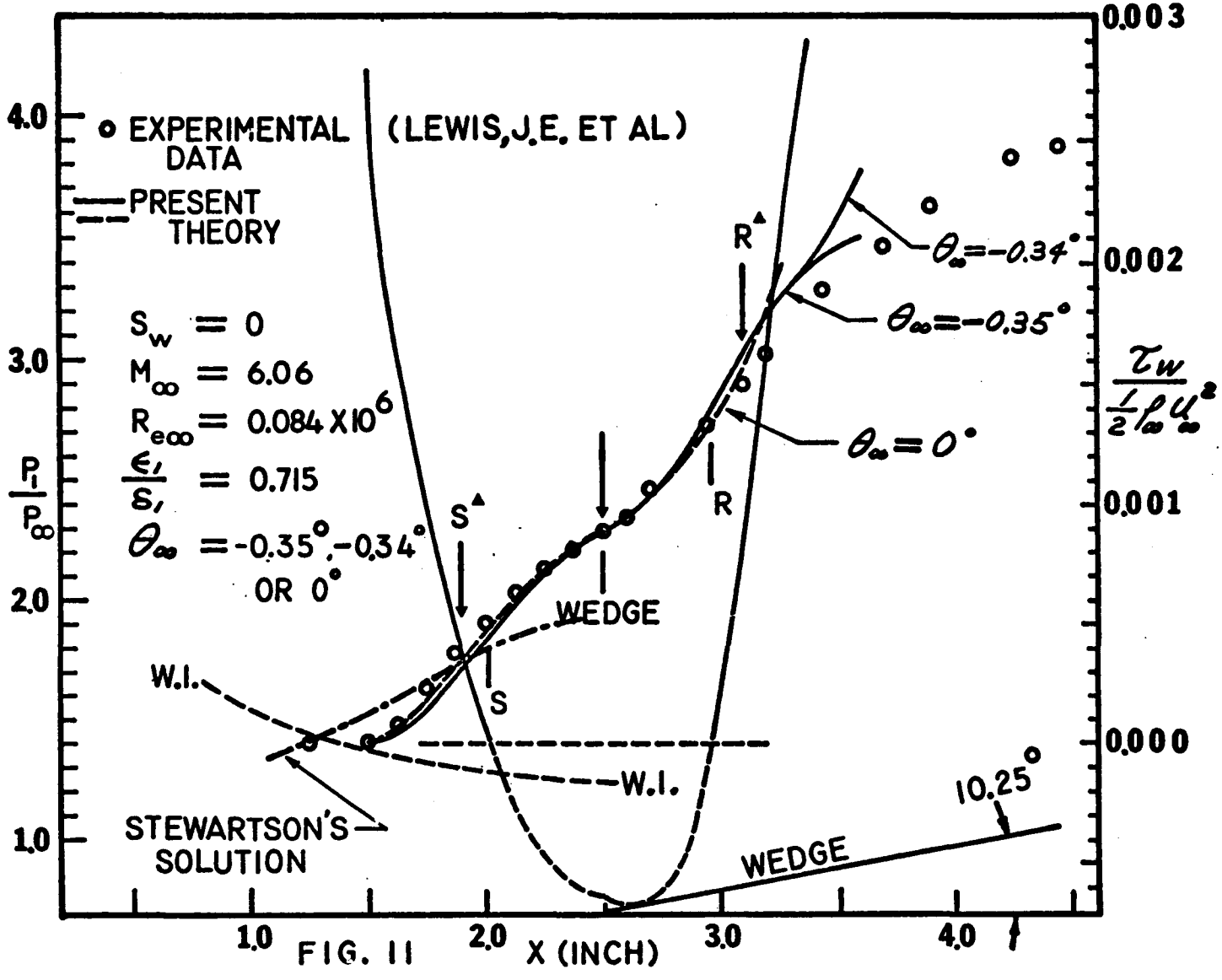
EXPERIMENTAL DATA (LEWIS, J.E. ET AL)
PRESENT THEORY
$S_w = 0$
$M_\infty = 6.06$
$R_{e\infty} = 0.084 \times 10^6$
$\frac{\epsilon_1}{\delta_1} = 0.715$
$\theta_\infty = -0.35°, -0.34°$ OR $0°$
$\frac{P_1}{P_\infty}$
$\frac{\tau_w}{\frac{1}{2}\rho_\infty U_\infty^2}$
4.0
3.0
2.0
1.0
0.003
0.002
0.001
0.000
S
R
$\theta_\infty = -0.34°$
$\theta_\infty = -0.35°$
$\theta_\infty = 0°$
WEDGE
W.I.
W.I.
STEWARTSON'S SOLUTION
10.25°
WEDGE
1.0
2.0
3.0
4.0
X (INCH)

FIG. 11

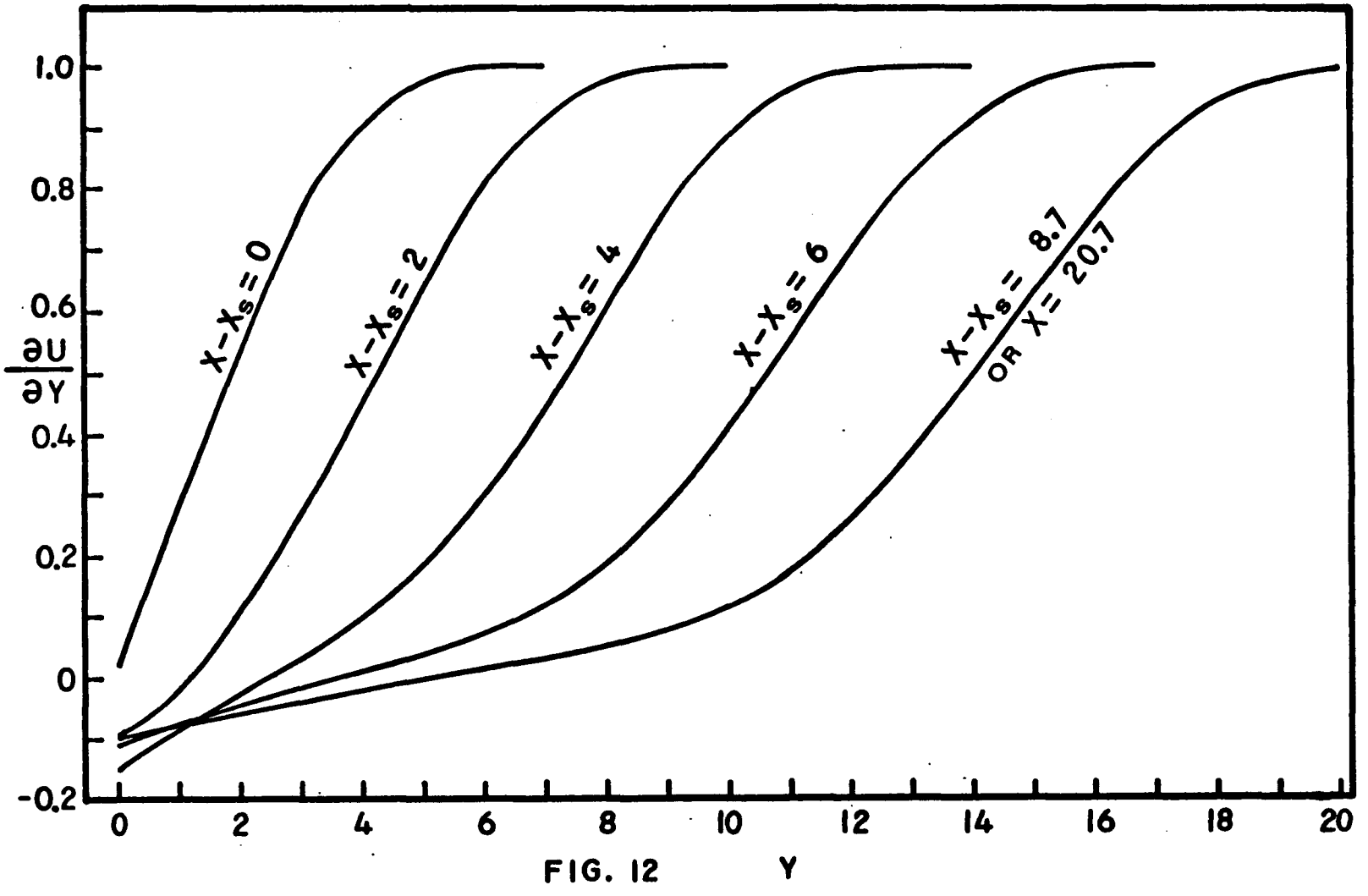
1.0
0.8
0.6
0.4
0.2
0
-0.2
∂U/∂Y
X-Xs=0
X-Xs=2
X-Xs=4
X-Xs=6
X-Xs= 8.7
OR X= 20.7
0
2
4
6
8
10
12
14
16
18
20
Y

FIG. 12

References

1. Baum, E., and Denison , M. R.,
" Interacting supersonic laminar wake calculations by a finite difference method ",
AIAA preprint 66-454, (1966).
2. Belcher, R. A., Burggraf, O. R., and Stewartson, K.,
J. Fluid Mechanics., 52 (1972), 753.
3. Blasius, H.,
" Grenzschichten in Flussigkeiten mit Kleiner Reibung ",
Zeitschrift fur Mathematik und Physik, Band 56, Heft 1, 1908, pp. 1-37.
4. Chapman, D. R., Kuehn, D. M., and Larson, H. K.,
" Investigation of separated flows in supersonic and subsonic streams with emphasis on the effect of transition ", Rept. 1356, 1958, NACA.
5. Cohen, C. B., and Reshotko, E.,
" Similar solutions for the compressible laminar boundary layer with heat transfer and pressure gradient ",
NASA Report 1293, (1956).
6. Crocco, L., and Lees, L.,
" A mixing theory for the interaction between dissipative flows and nearly isentropic streams ",
Journal of the Aeronautical Sciences, Vol. 19, No. 10, Oct. 1952, pp. 649-676.
7. Gadd, G. E.,
" A theoretical investigation of laminar separation in supersonic flow ", Journal of the Aero nautical Sciences, pp. 759-772, October 1957.
8. Garvine, R. W.,
" On upstream influence in Viscous interaction problems",
General Electric Co., Space Sciences Lab., R67SD41, (1967).

9. Georgeff, M. P.,
" A comparison of integral methods for the prediction of laminar boundary layer shock wave interaction ",
Imperial College Aero Report 72-01 (January 1972).
10. Gray, J. D.,
" On the existence of a pressure plateau in pure laminar separated flow ",
AIAA Journal Vol. 4, No. 9, Sept. 1966.
11. Hankey, W. L., Dwoyer, D. L., and Werle, M. J.,
" Branching solution for supersonic interacting boundary layer",
AIAA Journal, Vol. 11, pp 1349-51, September 1973.
12. Hayes, W. D., and Probstein, R. F.,
" Hypersonic flow theory ",
2nd Ed., Vol. 1. Academic Press, New York, 1966.
13. Holden, M. S.,
" An analytical study of separated flows induced by shock boundary layer interaction ",
Cal Report No. AI-1972-A-3 (December 1965).
14. Holden, M. S.,
" Theoretical and experimental studies of laminar flow separation on flat plate wedge compression surfaces in the hypersonic strong interaction regime ",
Cal Report No. AF-1894-A-2 (May 1967).
15. Klineberg, J. M. and Lees, L.,
" Theory of laminar viscid-inviscid interactions in supersonic flow ", AIAA Journal Vol. 7, No. 12, December 1969, pp. 2211-2221.
16. Lees, L. and Reeves, B. L.,
" Supersonic separated and reattaching laminar flows: 1. General theory and application to adiabatic boundary layer/shock wave interactions ",
AIAA Journal, Vol. 2, No. 11, Nov. 1964, pp. 1907-1920.

17. Lewis, J., Kubota, T., and Lees, L.,
" Experimental investigation of supersonic laminar, two dimensional boundary layer separation in a compressional corner with and without cooling ",
AIAA journal, Vol. 6, No. 1, Jan. 1968, pp. 7-14.
18. Ko, D. R. S. and Kubota, T.,
" Supersonic laminar boundary layer along a two dimensional adiabatic curved ramp ",
AIAA Journal, Vol. 7, No. 2, Feb. 1969, pp. 298-304.
19. Liepmann, H. W.,
" The interaction between boundary layer and shock waves in transonic flow ", Journal of the Aeronautical Sciences, Vol. 13, No. 12, Dec. 1946, pp. 623-637.
20. Liepman, N. W., and Roshtko, A.,
" Elements of gasdynamics ",
John Wiley and Sons (November 1957).
21. Lighthill, M. J.,
" On boundary layers and upstream influence, 1. a comparison between subsonic and supersonic flows ",
Proc. Roy. Soc. A, 217, 344-357 (1953).
22. Lighthill, M. J.,
" On boundary layers and upstream influence, 2. supersonic flows without separation ",
Proc. Roy, Sec. A. 217. 478-507 (1953).
23. Melnik, R. E. And Grossman, B.,
" Analysis of the interaction of a weak normal shock wave with a turbulent boundary layer ",
AIAA Paper No. 74-598, June 1974.
24. Mikhailov, V. V., Nieland, V. Ya., and Sychev, V. V.,
" The theory of viscous hypersonic flow ",
Annual review of fluid mechanics, Vol. 3, 1971.
25. Miller, D. S., Hyman, R., and Childs, M. E.,
" Mach 8 to 22 studies of separation due to deflected control surfaces ",
AIAA Journal Vol. 12 (Feb. 1964).

26. Nielsen, J. N., Lynes, L. L., and Goodwin, F. K.,
" Calculation of laminar separation with free interaction by the method of integral relations, Part 1 --- the two dimensional supersonic adiabatic flow, Cot. 1965. Part 2 --- two dimensional supersonic non-adiabatic flow and axisymmetric supersonic adiabatic and non-adiabatic flows ", Jan. 1966, AFFDL TR 65-107, Air Force Flight Dynamics Lab.
27. Neiland, V. Y., Izv. Akad. Nauk SSSR. Meh. Zidk.
28. Reyhner, T. A., and Flugge-Lotz, I.,
" The interaction of a shock wave with a laminar boundary layer ",
In ternational Journal of Non-linear Mechanics, Vol. 3, Pergamon Press, New York, 1968, pp. 173-199.
29. Rose, W. C.,
" Amethod for analyzing the interaction of an oblique shock wave and a boundary layer ",
Symposium on Analytic Methods in Aircraft Aerodynamics, NASA SP-228, Oct. 28-30, 1969, pp. 541-567.
30. Rose, W. C., Murphy, J. D., and Watson, E. C.,
" Interaction of an oblique shock wave with a turbulent boundary layer ",
AIAA Journal, Vol. 6, No. 9, Sept. 1968, pp. 1782-1783.
31. Rosenhead, L.,
" Laminar boundary layers ", Oxford 1963.
32. Schlichting,
" Boundary layer theory ", Fourth edition, Mcgraw-Hill 1955.
33. Sterret, J. R., and Emery, J. C.,
" Extension of boundary layer separation criteria to a Mach 6.5 by utilizing flat plates with forward-facing steps ", NASA TN D-618 (December 1960).

34. Sterrett, J. R. and Emery, J. C.,
" Experimental separation studies for two dimensional wedge and curved surfaces at M = 4.8 to 6.2 ",
TN D-1014, 1962, NASA.

35. Stewartson, K.,
" Further solutions of the Falkner-Skan equation ",
Proc. Comb. Phil. Soc., 50, 454-465, 1954.

36. Stewartson, K. and Williams, P. G.,
Mathematika, 20, (1973), 98-108.

37. Stollery, J. L. and Hankey, W. L.,
" Subcritical and supercritical boundary layers ",
AIAA Journal, Vol. 8, No. 7, pp. 1349-1351, July 1970.

38. Tani, I.,
" On the approximate solution of the laminar boundary layer equations ",
Journal Aero Sci., Vol. 21, No. 7, pp. 487-504, July 1954.

39. Weinbaum, S.,
" Rapid expansion of a supersonic boundary layer and its application to the near wake ",
AIAA Journal, 4, 217. 1966.

40. Weinbaum, S. and Goldburg, A.,
" The non-linear refraction of shock waves by upstream disturbances in steady supersonic flow ",
J. Fluid Mech. (1970), Vol. 43, part 1, pp. 1-33.

41. Weinbaum, S. and Garvine, R. W.,
" On the two dimensional viscous counterpart of the one dimensional sonic throat ",
J. Fluid Mech. (1969), Vol. 39, Part 1, pp. 57-85.

42. Werle, M. J., Polak, A., and Bertke, S. D.,
" Supersonic boundary layer separation and reattachment ---finite difference solutions ",
Report No. AFL 72-12-1, Dept. of Aerospace Engineering, University of Cincinnati, January 1973.

43. Werle, M. J., Dwoyer, C. L., and Hankey, W. L.,
" Laminar hypersonic interacting boundary layer: Subcritical branching in the strong interaction regime", ARL 72-0011, AD 741-759, Aerospace Research Labs. Wright-Patterson AFB, Ohio, February 1972.

44. Werle, M. J. and Vatsa, V. N.,
" Numerical solution of interacting supersonic boundary layer flows including separation effects ", ARL-73-0162, December 1973. Dept. of Aerospace Engineering, University of Cincinnati.

Vita

King-Mon Tu was born on June 30, 1940 in China. He received his undergraduate education at Nation Taiwan University and was granted the degree Bachelor of Mechanical Engineering in June, 1963. The author has served in the Chinese Army as a Second Lieutenant from July 1963 to July 1964. From September 1964 to July 1965, he attended graduate school as a full time student holding a scholarship at the University of Rochester and was granted the degree, Master of Science in June 1966. During the period from July 1965 to August 1966, he was employed by Graflex Inc. as a Design Engineer in the Engineering Development Section working on Audio-Visual Instruments. In September 1966, he attended New York University as a full time student and was holding a graduate assistantship until June 1969. King-Mon Tu began full time study toward a Doctor of Philosophy in Mechanical Engineering Thermal and Fluid Sciences in June 1969 at the City University of New York. He has been supported by a City University Research Assistantship from June 1969 till August 1973. He also worked as a part time lecturer in the Mechanical Engineering Department of the City College of New York during the Fall semester of 1973 and the Spring semester of 1974. The author also holds the rank of Associate Menbership in the AIAA.